

Factors controlling atmospheric DMS and its oxidation products (MSA and nssSO₄²⁻) in the aerosol at Terra Nova Bay, Antarctica

Silvia Becagli^{1,2}, Elena Barbaro², Simone Bonamano³, Laura Caiazzo¹, Alcide di Sarra⁴, Matteo Feltracco², Paolo Grigioni⁴, Jost Heintzenberg⁵, Luigi Lazzara⁶, Michel Legrand⁷, Alice Madonia³, Marco Marcelli³, Chiara Melillo⁶, Daniela Meloni⁴, Caterina Nuccio⁶, Giandomenico Pace⁴, Ki-Tae Park⁸, Suzanne Preunkert⁷, Mirko Severi^{1,2}, Marco Vecchiato², Roberta Zangrando² and Rita Traversi^{1,2}

¹Department of Chemistry “Ugo Schiff”, University of Florence, Sesto F.no (FI), 50019, Italy.

²Intitute of Polar Sciences, National Research Council (CNR-ISP), Venice Mestre (VE), 30172, Italy

³Department of Ecologic and Biologic Science, University of Tuscia, Civitavecchia, 00053, Italy.

10 ⁴ENEA Laboratory of Observations And Measurements for the environment and climate, Rome, Italy

⁵Leibniz-Institute for Tropospheric Research, Leipzig, 04318, Germany.

⁶Department of Biology, University of Florence, 50121, Florence, Italy

⁷IGE-Institute des Géosciences de l’Environnement, S. Martin d’Heres, 38400, France

⁸Korea Polar Research Institute (KOPRI), Incheon 406-840, South Korea.

15 *Correspondence to:* Silvia Becagli (silvia.becagli@unifi.it)

Abstract. This paper presents the results of simultaneous high time resolution measurements of biogenic aerosol (methane sulfonic acid-MSA, non-sea salt sulfate nssSO₄²⁻) with its gaseous precursor dimethylsulfide (DMS) performed at the Italian coastal base Mario Zucchelli Station (MZS) in Terra Nova Bay (MZS) during two summer campaigns (2018-2019 and 2019-2020). The study provides information on marine biological activity in the nearby polynya in the Ross Sea and on the influence of biogenic and atmospheric processes on biogenic aerosol formation. Data on atmospheric DMS concentration are scarce especially in Antarctica. The DMS-maximum at MZS occurs in December, one month earlier than at other Antarctic stations. The maximum of DMS concentration is connected with the phytoplanktonic senescent phase following the bloom of *Phaeocystis antarctica* that occurs in the polynya when sea ice opens up. The second plankton bloom occurs in January and, despite the high Dimethylsulfopropionate (DMSP) concentration in sea water, atmospheric DMS remains low probably due to its fast biological turnover in sea water in this period. The intensity and timing of the DMS evolution during the two years suggests that only the portion of the polynya close to the sampling site produces a discernible effect on the measured DMS. The closeness to the DMS source area, and the occurrence of air masses containing DMS and freshly formed oxidation products allow to study the kinetic of biogenic aerosol formation and the reliable derivation of the branch ratio between MSA and nssSO₄²⁻ from DMS oxidation that is estimated to be 0.84 ± 0.06. Conversely, for aged airmasses with low DMS content, an enrichment of nssSO₄²⁻ with respect to MSA, due to the presence of background concentration of nssSO₄²⁻ from volcanic origin (Erebus) or formed from MSA oxidation in aqueous phase during the transport.. Therefore, the aged air mass presents an MSA/nssSO₄²⁻ ratio lower than in newly formed biogenic aerosol. By considering the sum of MSA and biogenic nssSO₄²⁻, we estimate that the mean contribution of biogenic particulate matter to PM₁₀ is 17%, with a maximum of 56%. The high contribution of biogenic aerosol to the total PM₁₀ mass in summer in this area highlights the dominant role of the polynya on

35 biogenic aerosol formation. Finally, due to the regional and year-to year variability of DMS and related biogenic aerosol formation, we stress the need for long-term measurements of sea water and atmospheric DMS and biogenic aerosol along the Antarctic coast and in the Southern Ocean.

1 Introduction

Dimethylsulfide (DMS) is a volatile organic sulfur compound produced in surface oceanic waters all over the world characterized by low solubility in water. DMS is formed by the breakdown of the dimethylsulfoniopropionate (DMSP), a phytoplankton metabolite (Stefels, 2000). In surface waters, substantial quantities of dissolved DMSP and DMS can be detected, but another important sulfur cycle compound in sea water is dimethyl sulfoxide (DMSO) whose concentrations exceeds the concentration of DMS and DMSP (Asher et al., 2017). DMSO is mainly produced from photochemical and bacterial DMS oxidation, the latter process may serve as an energy source for bacteria (Bodein et al., 2011). The loss processes of dissolved DMS include (i) microbial consumption, (ii) photooxidation, (iii) air-sea gas exchange and (iv) vertical export by mixing (Simo, 2004). In particular, approximately 10% of total global DMS production ventilates through the sea-air interface (Simó et al., 1999; Simó and Pedrós-Alió, 1999) to the atmosphere, where it accounts for approximately 50% of the natural global sulfate burden (Simó, 2001). The global DMS flux to the atmosphere is currently estimated to be 28.1 (17.6–34.4) Tg S per year, which is approximately half the anthropogenic global atmospheric sulfur input (Klimont et al., 2013; Hulswar et al., 2021). This makes DMS an important contributor to global sulfur fluxes. Once in the atmosphere, DMS is oxidized both in gas and water phase by O_3 or by the hydroxyl (OH), nitrate (NO_3), chlorine (Cl), and bromine oxide (BrO) radicals to form either methanesulfonic acid (MSA) or sulfur dioxide (SO_2), which is further oxidized to H_2SO_4 (Gondwe et al., 2003; Read et al., 2008; Fung et al., 2022). The production of sulfuric acid and MSA (having low vapor pressure) may lead to new particles formation (NPF) when few particles condensation nuclei are available (Dall'Osto et al., 2017). NPF linked to DMS products may play a fundamental role in the polar regions, with possible effects on climate (Dall'Osto et al., 2017). The growth of particles following NPF is crucial in generating cloud condensation nuclei (CCN), which eventually allow the formation of cloud drops. As CCN are important for cloud formation and thereby indirectly affect the radiation balance, they have an important climatic impact and are involved in feedback processes (Charlson et al., 1987). Actually, there are still large uncertainties in both the sign and the amplitude of this feedback (Quinn and Bates, 2011). Besides, model calculations of the future response of DMS to changes in global temperature vary widely: both increases (Cameron-Smith et al., 2011; Gabric et al., 2005; Qu et al., 2021; Wingenter et al., 2007), and decreases (Kloster, 2007) in surface water DMS concentrations have been predicted.

DMS concentrations global climatology shows that the polar regions are of significant importance to the total global DMS production, in particular the Southern Ocean (Gondwe et al., 2003; Hulswar et al., 2021). The total annual Southern Ocean (south of 40°S) DMS flux is estimated at approximately 5.8 Tg S (Hulswar et al., 2021). Most of the DMS emission, 3.4 Tg S (Jarníková et al., 2016), occurs during summer months (December to February).

The link between climate change and DMS production is complex and involves a great number of oceanic and atmospheric processes: in polar region the maximum DMS concentrations in the water occurs in early summer and is primarily associated with sea-ice break-up (Stefels et al., 2018). Although the retreat in sea ice will directly impact on the release of DMSP and
70 DMSP-producing algae, changes in the physical environment can also indirectly impact on phytoplankton productivity and composition through changes in light and nutrient availability (Ducklow et al., 2007; Montes-Hugo et al., 2009).

Wind speed plays a relevant role in DMS production in the ocean and in regulating the flux from the ocean. The depth of the oceanic mixed layer, largely influenced by wind, is crucial for the determination of oceanic DMS distribution: for example, a high wintertime ice extent can shield the water column from high wind speeds, thus preventing the deepening of the winter
75 mixed layer. Declining wind speeds in summer can cause the persistence of a shallower mixed layer depths, and when these variables coincide with the seasonal summertime increase in light availability for primary production, high DMS summer maxima are observed (Saba et al., 2014). Similarly, high summertime winds or a shorter duration of the sea ice season along the marginal ice zone can lead to lower summertime chlorophyll-a (Chl-a) maximum as the mixed layer is deeper, thereby inhibiting algal cells from overcoming light limitation.

Besides processes in the water column, ocean-air DMS flux has a more of a linear relationship with wind speed, as it is largely transported by interfacial exchange and it is not as influenced by bubbles (i.e. whitecaps, Bell et al., 2017; Zavarisky et al., 2018) as other more insoluble gases. Vlahos and Monahan (2009) evidenced that at wind speed higher than 10 m/sec DMS transfer rates decreases due to the amphiphilic nature of DMS that leads to transfer delay because higher wind speeds cause a higher concentration of sinking bubbles by whitecapping of the ocean surface. Anyway, Marandino et al. (2007) demonstrate
85 that most of the variance in the fluxes can be accounted by variations in DMS sea surface concentration (37%) than wind speed (19%).

Several studies tried to correlate DMS concentrations in sea water and algal biomass from surface and satellite data, but contradictory results have been found : positive (Andreae and Barnard, 1984; Belviso et al., 2004; Leck et al., 1990), negative (Froelich et al., 1985; Watanabe et al., 1995), as well as absent (Barnard et al., 1984; Deng et al., 2021) correlations were
90 found. Such uncertain relationships affect the calculation of DMS flux based on the algal biomass. In most models, the DMS fluxes are obtained from small or medium scale field observations (Gabric et al., 2014; Kloster et al., 2006) making our understanding of the mechanisms controlling DMS emissions regionally dependent; however, some regions of the Southern Ocean are not covered by measurements, making these estimates unpractical.

Especially, data on DMS concentrations in the Ross Sea are scarce, and atmospheric DMS observations are missing. Actually,
95 the study of DMS production and its fate in the atmosphere is relevant in this area due to the presence of a persistent polynya. Polynyas are areas of seasonally open water surrounded by sea ice in high latitude regions. They are characterized by abundance of macronutrients, an ample supply of iron (Fe) from melting sea ice and/or glaciers and continental shelf sediments resulting from the intrusion of relatively warm, salty, and nutrient-rich Circumpolar Deep Water (Arrigo et al., 2012; Sherrell et al., 2015; St-Laurent et al., 2017). Consequently, they often exhibit high primary productivity (Arrigo et al., 2012; Arrigo
100 and van Dijken, 2003; Yager et al., 2012) because they are the first polar marine systems to be exposed to the increasing

springtime solar radiation (Arrigo and van Dijken, 2003; Criscitiello et al., 2013). The polynyas in the Southern Ocean are the most productive biological regions and have the highest DMS sea–air flux in the world (Hulswar et al., 2021). DMS concentrations as high as several hundred nanomoles per litre have been observed in polynyas along the coastal regions of Antarctica, such as the Ross Sea and Amundsen Sea (Tortell et al., 2012; del Valle et al., 2009) where there are the favourable conditions for *Phaeocystis antarctica* blooms (Oliver et al., 2020).

Finally, the large uncertainty in the processes surrounding DMS production emphasizes the need for an improved mechanistic understanding and model parameterization of the atmospheric DMS. However, measurements of DMS in the atmosphere are scarce and especially in coastal Antarctica because of the difficulty in conducting a field observation in these extreme environments. Therefore, the sources and the evolution of the aerosol over the Antarctic are still a subject of many open questions. It is necessary to fill the data gap in the knowledge of biogenically-derived aerosols (both secondary inorganic and primary organics) in the Antarctic to improve understanding of the effects of ocean ecosystem on the marine aerosol-cloud-climate system.

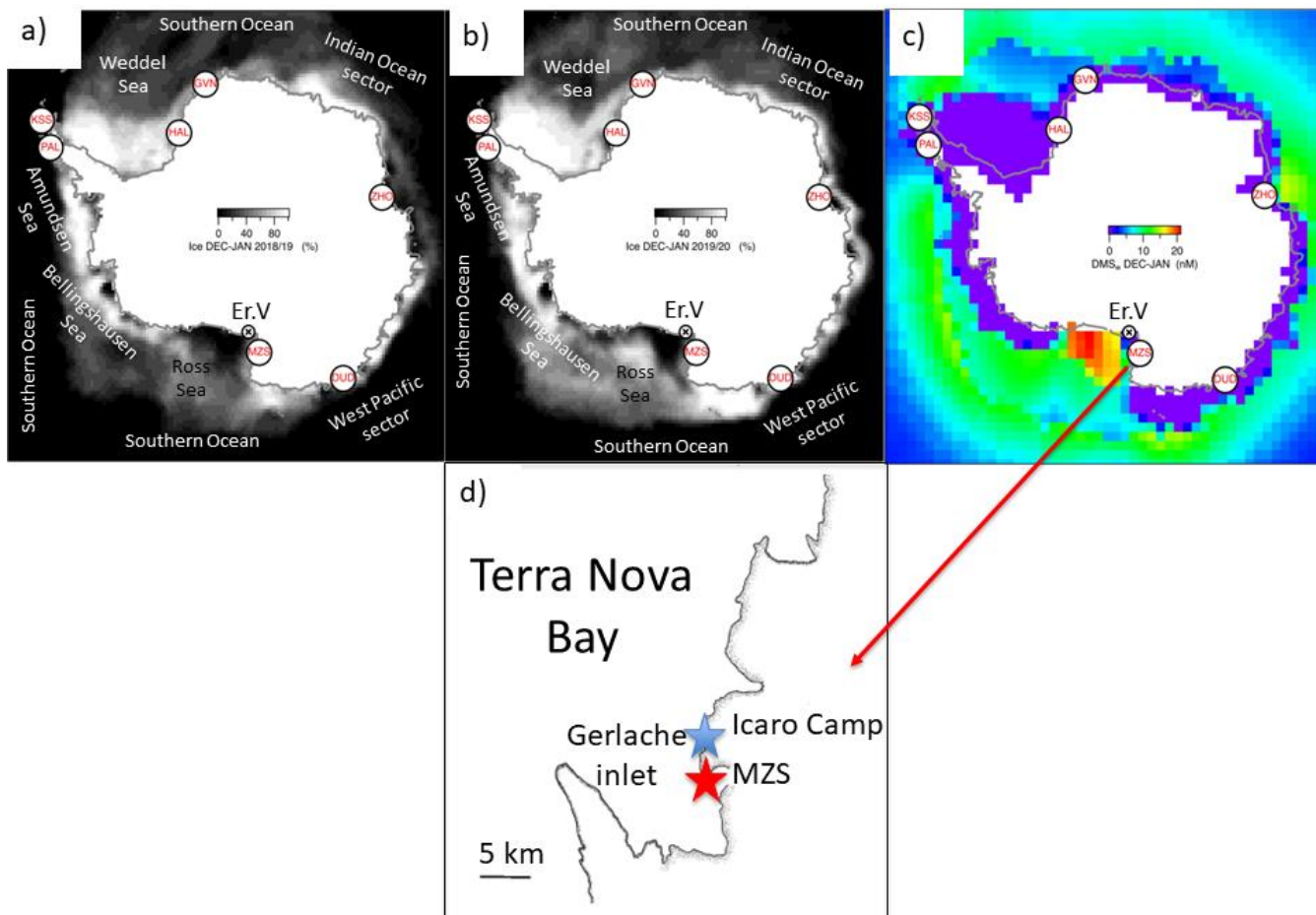
In this study we report high resolution (12h) measurements of MSA and nssSO_4^{2-} in the particle phase simultaneous to gas phase DMS obtained for the first time in Northern Victoria Land, at the Mario Zucchelli Station (MZS) facing the polynya area in the Ross Sea.

This work gives new hints to enhance our knowledge of the interactions between oceanographic parameters, the surface ocean biosphere, and biogenic aerosol formation in this region of our planet.

2. Methods

2.1 Sampling area

Aerosol and DMS sampling are performed in two Antarctic summer campaigns (AC): 2018-2019 and 2019-2020. The campaigns lasted from the beginning of November until to the end of January in the area surrounding the Antarctic Italian base Mario Zucchelli Station (MZS – 74°42' S, 164°07' E) located at Terra Nova Bay, along the coast of the Northern Foothills to north-east of Gherlache Inlet (Fig. 1). There is a persistent polynya in the sea facing the base, the extent of which is shown in the average ice maps for the two campaigns (Fig. 1). Fig. 1 also includes average DMS concentrations (nM) in surface waters for the period December-January according to the climatology of (Hulswar et al., 2021).



130 **Figure 1.** Average sea ice cover during campaign 2018-19 (a), and 2019-2020 (b) with sea ice data from NSIDC (<https://nsidc.org>, last accessed 2021.11.04); c) average DMS (nM) in surface waters during December-January according to the DMS climatology of (Hulswar et al., 2021). Figure on the bottom (d) reports the enlarged map of the Terra Nova Bay with Mario Zucchelli Station (MZS- red star) and the aerosol samplings site (Campo Icaro- light blue star). The geographical location of the volcano Erebus (Er.V) and the Antarctic stations reported in Table 1 are reported in figure (a), (b) and (c).

2.2 Aerosol sampling and analysis

In order to avoid possible contamination from the base, the site chosen for aerosol sampling is Icaro Camp (74° 42' 43"S 164° 07' 00"E) located about 2 km south of MZS. The aerosol sampler was installed on the hill facing the sea at about 30m above sea level.

135

Aerosol sampling was performed at 12 h resolution by a low volume sequential aerosol sampler (Giano – Dado lab srl Milano) equipped with PM₁₀ sampling head operating at constant air flow of 2.3m³/h in accord with the European rule EN12341.

Aerosol samples were collected on Teflon filters (PALL, Germany), 47 mm in diameter, with 2.0 μm nominal porosity and 99.5 % sampling efficiency for 0.3 μm aerodynamic particle diameter. The filters were shipped to Italy, being kept at $-20\text{ }^{\circ}\text{C}$,
140 and stored in Petri plastic dishes, until they are cut, extracted, and analyzed.

In the laboratory the PM_{10} mass was determined by weighting filters before and after the sampling on a 5-digit microanalytical balance (Sartorius) equipped with an ionic cannon to avoid mass fluctuations due to the electrostatic charge of filters. Before weighting, filters were stored in a dryer for 48 h, with $50 \pm 5\%$ relative humidity. A fourth of each filter was devoted to the ion determination by ion chromatography (IC). The $\frac{1}{4}$ filter was extracted in ultrapure water (Resistivity $> 18\text{ M}\Omega$) in an
145 ultrasonic bath at room temperature, then the ionic content was determined by three ion chromatographs (two ICS-1000 and one DX500 Thermo Fisher Scientific Inc., USA) equipped with Gilson 222 XL autosampler. This system makes it possible to simultaneously determine both anions (inorganic and selected low molecular weight organic anions) and cations within 10 min. Details on IC measurements are reported in (Becagli et al., 2022).

In order to exclude the sea salt contribution to the total SO_4^{2-} budget, the non-sea salt (nss) SO_4^{2-} was calculated as follows:

$$150 \text{ nssSO}_4^{2-} = \text{SO}_4^{2-} - (\text{SO}_4^{2-}/\text{Na}^+)_{\text{sw}} * \text{Na}^+$$

where SO_4^{2-} and Na^+ are the measured concentrations in the aerosol samples (as ng/m^3) and $(\text{SO}_4^{2-}/\text{Na}^+)_{\text{sw}}$ is the SO_4^{2-} to Na^+ ratio in sea water 0.25 w/w (Henderson and Henderson, 2009).

2.3 Gaseous DMS sampling and analysis

DMS sampling is performed near the main MZS building at about 5 m distance from the sea at 2 m above sea level. The
155 sampling was done at sub daily resolution (typically 4 samples in 24 hours) by filling electropolished stainless steel canisters by compressing the air at 4 bars within several minutes with a membrane pump (Millipore XX5522050). Before sampling, the canister was filled and emptied two times with ambient air in order to wash the canister avoiding memory effects from the previous samples.

DMS measurements were made in the MZS laboratories by using a gas chromatograph equipped with a flame photometric
160 detector (HP6890, 393 nm). DMS is trapped in an ethanol bath at -70°C on a porous polymer resin based on 2,6-diphenylene oxide (Tenax®) contained in a sample loop. DMS is injected in the GC by thermal desorption in boiling water. Working conditions are reported in detail by Legrand et al. (2001). Daily calibrations were achieved by using a permeation tube (VICI Metronics, Santa Clara California) thermostated at 30°C . The permeation tube was calibrated, and its stability was checked, resulting in less than 5% changes within one year (Preunkert et al., 2007). The limit of quantification (LOQ) is 0.2 ng, leading
165 to an atmospheric detection limit of 12 pptV for the 6 L volume of air usually trapped into the Tenax®. In order to reduce the LOQ high amount of air (up to 25 L) is trapped into the Tenax® at the beginning of the field campaign when DMS concentration was low.

2.4 DMSP in sea water sampling and analysis

During both ACs sea water samples were collected at the sea surface in two sites about once a week, when the piers were free from sea ice and meteorological condition allowed to use a boat. The two sampling sites were chosen in ice free water about 2 miles from the coast and from the sea ice margin and 2 miles from each other. Few samples in November 2018 were collected in a hole in the pack ice, about 1 km from MZS in the Gerlache Inlet. The samples were collected in Schott® bottles, acidified to pH <2 by adding small amount of distilled HNO₃, then hermetically sealed, and maintained at 4°C until the analysis. The analysis was accomplished at the Korea Polar Research Institute (KOPRI) laboratories. The preserved DMSP sample was hydrolyzed to gaseous DMS using 10 M NaOH (addition of 0.25 mL per mL sample) and was allowed to react overnight in the dark. Then, DMS was measured by using a gas chromatography equipped with pulsed flame photometric detector (GC-PFPD) as described in (Park et al., 2014). The DMSP sample was measured in duplicate, and the analytical precision was generally better than 5%.

2.5 UV-A and SW irradiance measurements

Measurements of downwelling photosynthetically active radiation and shortwave irradiance were made at Icaro Camp throughout 2018-2019 and 2019-2020. Measurements of UV-A and UV-B irradiances were added during the 2019-2020. The shortwave irradiance was measured with a compact Kipp and Zonen Splitte sensor, while the photosynthetically active radiation (PAR) with a Li-cor 190R. Both instruments were calibrated by the manufacturer before deployment. In additions, the radiometers were installed at the Lampedusa Climate Observatory before deployments in Antarctica in 2018 and 2019, where they were compared with instruments continuously running at the site. The calibration of the shortwave irradiance radiometers at Lampedusa is traceable to the World Meteorological Organization World Radiation Reference scale (e.g., di Sarra et al., 2019). The PAR calibration scale has been maintained at Lampedusa relying on the initial manufacturer calibration and on the local calibration of a multi-band radiometer through the Langley plot method (Trisolino et al., 2017).

A UV-A and a UV-B broadband radiometer, a Delta-T UV2/ap and UV2/bp, respectively, were added for the 2019-2020 AC. The radiometers were calibrated at Lampedusa before the campaign by comparison with measurements of spectral irradiance performed with a double monochromator Brewer spectrometer. Nominal spectral response functions (peaked respectively at 373 and 313 nm for the UV-A and UV-B, corresponding bandwidths of about 31 and 26 nm) were used in the determination of the broadband calibration. The Brewer spectrophotometer is regularly calibrated on site with 1000 W FEL lamps (Di Sarra et al., 2008).

2.6 Wind Speed and direction data

Wind speed and direction data were measured at Eneide automatic weather station (AWS) (74° 41' 45"S 164° 5' 32"E) that takes part of the Meteo-Climatological Observatory at MZS and Victoria Land maintained by the Italian National Programme

of Antarctic Research (<http://www.climantartide.it>). This AWS is nearest to both the DMS and aerosol sampling sites and it have been used in this work.

200 **2.7 Satellite data of sea ice and Chlorophyll**

Daily maps of southern hemisphere sea ice cover were obtained from the National Snow & Ice Data Center. Information on sea ice extent is derived from the analysis of satellite passive microwave brightness temperature data from the Nimbus-7 Scanning Multichannel Microwave Radiometer (SMMR) and from a series of Special Sensor Microwave Imager (SSM/I) and Special Sensor Microwave Imager/Sounder (SSMIS) instruments (Fetterer et al., 2017). The nominal spatial resolution is 205 25x25 km². Data were downloaded from <https://nsidc.org/data> (last accessed 2021-12-22).

Satellite-derived daily L3 data sets of surface Chlorophyll-a concentration with a 4km spatial resolution from the European Space Agency's GlobColour Project (<http://hermes.acri.fr>) were obtained from the Copernicus Marine Environment Monitoring Service (CMEMS, <https://marine.copernicus.eu/>). The Chl-a product is derived by reprocessing the merged observations from five satellite radiometers (MODIS on Aqua, VIIRS from Suomi-NPP and JPSS-1, and OLCI from Sentinel 210 3a and 3b). The GlobColour dataset is a common and appropriate choice for phytoplankton dynamics studies even in the Southern Ocean (Ardyna et al., 2017; Cole et al., 2015).

2.8 Backward trajectories calculation

Ten-day back trajectories are calculated with the HYSPLIT-model (Stein et al., 2015). We used the ensemble method of the model that has been incorporated directly into the code so that trajectories are automatically computed about a 3-dimensional 215 cube about the starting point at 300 m above MZS. The initial positions are not offset, just the meteorological data point associated with each particular trajectory, so that all trajectories start from the same point (https://www.ready.noaa.gov/documents/Tutorial/html/traj_ensem.html, last accesses 2021-12-22). The trajectories are based on the meteorological fields of the Global Data Assimilation System (GDAS1) provided by the US National Weather Service's National Centers for Environmental Prediction (NCEP) at one-degree resolution (<https://www.ready.noaa.gov/gdas1.php>, last 220 accesses 2021-12-22).

3. Result and discussion

Fig. 2 shows the time series of DMS, MSA and nssSO₄²⁻ concentrations during the two summer Antarctic campaigns. In order 225 to derive the stoichiometric ratio between the two aerosol species (MSA and nssSO₄²⁻) and its gaseous precursor (DMS) the concentrations are reported in nMol/m³.

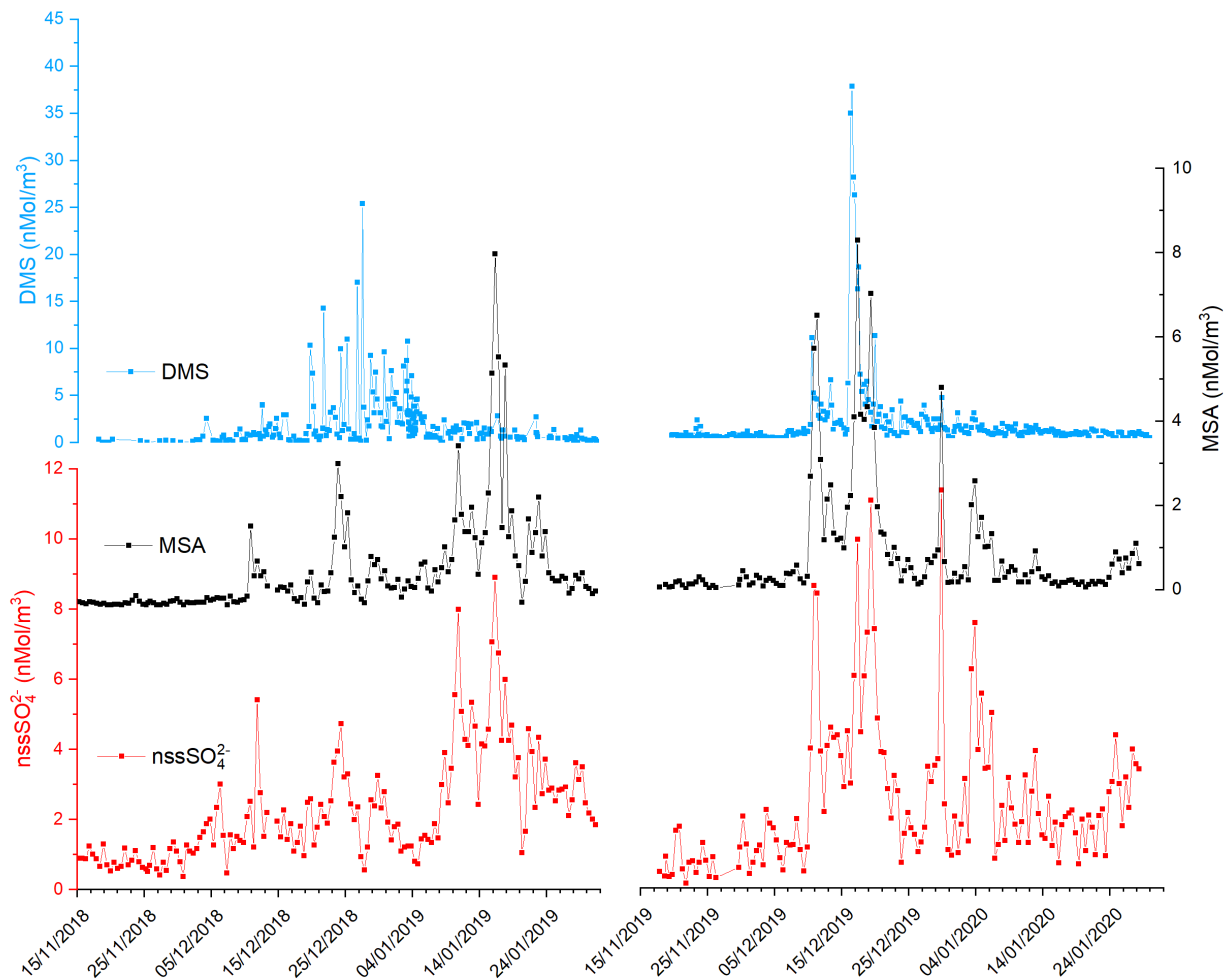


Figure 2. Time series of DMS, MSA and nssSO_4^{2-} in the two AC: 2018-19 (plots on the left) and 2019-20 (plot on the right).

230

The three compounds display very different pattern in the two summer ACs, as concerns timing and concentration maxima. During the 2018-19 AC the DMS concentration maxima are lower but last longer than in the 2019-20 campaign. The median and 75° percentile of the DMS concentration measured in the two ACs are 0.67 and 1.81 nMol/m³, respectively. DMS values higher than the 75° percentile occurred during 27%, and 17% of the time for the 2018-19 AC and 2019-20 AC, respectively, although the maximum DMS concentration was lower (25.4 nMol/m³) in the 2018-19 AC than in the 2019-20 AC (37.7 nMol/m³). Basic statistics on the measured values of DMS, MSA, and nssSO_4^{2-} in the two ACs are reported in Table 2, and are compared with measurements performed at other Antarctic sites and over the Southern Ocean. Biogenic aerosol data from Antarctic sites and the Southern Ocean are scarce, and even more so for measurements of DMS. However, despite a general spatial (site to site) and temporal (year to year at the same site) variability some considerations can be made. Despite its more

235

240 southern position, the maximum DMS concentration at MZS occurs earlier (December) than at DDU and over the Southern
 Ocean (January). This is likely due to the influence of the polynya, where an early phytoplanktonic bloom, and consequently
 an early release of DMS to the atmosphere from the ice-free area, takes place. However, notwithstanding the large year to
 year variability, the DMS summer mean and maximum concentration at MZS are lower than at the other sites reported in Table
 1. Maximum concentrations of MSA and nssSO_4^{2-} at MZS occur in December (in correspondence with the DMS maxima) or
 245 in January. The MSA and nssSO_4^{2-} peaks coincide largely with those of its precursor DMS. However, the DMS number of
 moles is always larger than that of MSA and nssSO_4^{2-} . The DMS life time in summer in Antarctica is modelled to be in the
 range 0.5-3 days (Faloona, 2009; Hezel et al., 2011; Fung et al., 2022). Consequently, we assume that the measured DMS
 comes from the open ocean areas near the sampling site and is not yet fully oxidized.

Although MSA concentrations show a high site-to-site variability, it appears that at MZS, MSA concentrations are higher than
 250 at the other sites reported in Table 1. Non sea salt SO_4^{2-} values at MZS are of the same order of magnitude as at the other
 Antarctic sites, except at Halley and on the ocean cruise, where smaller concentrations are found.

Table 1. Mean and standard deviation of DMS, MSA and nssSO_4^{2-} concentrations in coastal Antarctic sites. § summer mean calculated
 over the years 1999-2003; * summer mean calculated over the years 1997/98, 2001/02,2002/03; ° summer mean calculated over the years
 255 1996/97, 1999/00, 2001/02.

Station	Coord.	Year	Month	DMS (gas phase)		MSA (aerosol)		nssSO_4^{2-} (aerosol)		Reference
				Mean (std dev) nMol/m ³	Max nMol/m ³	Mean (std dev) nMol/m ³	Max nMol/m ³	Mean (std dev) nMol/m ³	Max nMol/m ³	
MZS	74°42' S, 164°07' E	2018- 19	Dec	2.32 (3.87)	25.4	0.60 (0.65)	3.41	2.02 (0.93)	5.41	this work
MZS	74°42' S, 164°07' E		Jan	1.78 (1.88)	10.7	1.47 (1.53)	8.4	3.41 (1.75)	8.90	this work
MZS	74°42' S, 164°07' E	2019- 20	Dec	2.90 (5.98)	37.7	1.50 (1.88)	8.29	3.19 (2.58)	11.3	this work
MZS	74°42' S, 164°07' E		Jan	0.61 (0.49)	2.7	0.51 (0.50)	2.58	2.46 (1.39)	7.55	this work
DDU	66°40'S, 140°01'E	1998- 99	Jan	13.10 (6.10)		0.60 (0.30)		3.80 (1.4)		(Jourdain and Legrand, 2001)

Neumayer		1983-95	Jan			1.60 (0.80)		3.95 (1.39)		(Minikin et al., 1998)
DDU	66°40'S, 140°01'E	1991-95	Jan			0.66 (0.20)		3.57 (0.41)		(Minikin et al., 1998)
Halley	73°35'S 26°19'W	1991-93	Jan			0.35 (0.21)		0.93 (0.37)		(Minikin et al., 1998)
DDU	66°40'S, 140°01'E	1991-2003	summer	8.2§	227.2§	0.36* 0.76°		1.89* 2.57°		(Preunkert et al., 2007)
Palmer	67.77S, 64.05W	1994	Jan-Feb	4.92 (3.89)		1.76 (1.42)		2.85 (2.24)		Barrensheim et al., 1998
Halley	73°35'S 26°19'W	2004	Jan-Feb			0.87				(Read et al., 2008)
Halley	73°35'S 26°19'W	2005	Jan-Feb			1.47				(Read et al., 2008)
Zhongshan	69°22'S 76°22'E	2005-2008	Jan-Mar			0.46- 0.87		1.17- 2.43		(Zhang et al., 2015)
Cruise in Southern Ocean	40°S-76°S; 170°E - 110°W	2018	Feb-Mar	36.8 (39.2)	445.4	0.32		1.54 (0.34)		(Yan et al., 2020)
King Sejong	62.2° S, 58.8° W	2018-2020	Dec-Mar	1.79 (1.50)	24.3	1.00 (0.34)	2.05	2.35 (1.01)	5.82	(Jang et al., 2022)

3.1 Factors controlling atmospheric DMS: wind speed and direction, Chl and sea ice extent

260 The difference between the DMS evolution in ACs 2018-2019 and 2019-2020 shown in Fig. 2 may be due to different causes: biological (DMS production from phytoplankton), physical (DMS flux from sea water to the atmosphere), or chemical (different rates of DMS oxidation in the atmosphere).

The role of wind speed has been firstly investigated. The DMS sea air flux depends on oceanic DMS concentrations and on the transfer velocity coefficient (k_w), which is a function of wind speed (Nightingale et al., 2000; Vlahos and Monahan, 2009; 265 Bell et al., 2017; Zavarsky et al., 2018). Moreover, the measured DMS atmospheric concentrations at coastal sites are expected to be heavily influenced by the wind direction, as DMS sea-to-air transfer occurs only at the ice-free ocean surface, and air masses coming from the ice sheet do not contain DMS.

In the AWS hourly data set wind coming from the continental ice sheet, i.e., wind direction between 200 and 350°, were identified in the period 6 December-6 January when maximum DMS release in the atmosphere is measured in both campaigns.

270 Surprising, the fraction of time with winds blowing from the ice-sheet is higher in 6 Dec. 2018 - 6 Jan.2019 (when more

samplings with DMS concentration > 75th percentile are observed) than 6 Dec. 2019 - 6 Jan. 2020 (68% and 48% of time respectively, see Table 2), suggesting that the different evolution of the DMS concentration is not produced by a different pattern of wind direction.

275 Data display conversely a dependency on wind speed. The distribution of wind speeds for cases with high DMS concentrations (> 75th percentile) displays that the 82-83% of wind speeds are in the range 1-10 m/sec in the two campaigns.

This is consistent with modeled DMS transfer rate as function of wind speed that increases as wind speed increases up to 10 m/sec but decreases as wind speed increases (Vlahos and Monahan, 2009).

280 If we consider the wind speed velocity in the range 1-10 m/sec as the best conditions for DMS transfer rate, by looking at the wind distribution in the above mentioned time period for the two year we can see an opposite pattern than expected with lower percentage of favorable wind speed in the year with higher number of DMS concentration higher than 75th percentile (table 2).

Table 2. Number of data and percentage of DMS concentration higher than 75th percentile, wind direction from the ice sheet and wind speed lower than 10 m/sec.

	DMS conc. >75 th percentile		Wind Direction from the ice sheet		Wind speed <10 m/sec	
	n. of data	%	n. of data	%	n. of data	%
6 Dec. 2018-6 Jan.2019	63	42	525	68	425	55
6 Dec. 2019-6 Jan.2020	49	38	366	48	569	74

285

Therefore, large differences in the DMS sea to air transfer velocity do not seem to occur, and are not expected to be the cause of the different behavior of DMS evolution in the two ACs. Unfortunately, we do not have measurements of DMS in sea water, that could have confirmed this hypothesis, but it is consistent with previous modeling and experimental evidences assessing that the large year-to-year variability of atmospheric DMS concentrations can not be explained by changes of meteorological processes controlling the k_w factor or by changes of atmospheric oxidants, but most likely by changes in oceanic DMS concentrations (Sciare et al., 2000; Kettle and Andreae, 2000; Marandino et al., 2007; Bock et al., 2021).

290

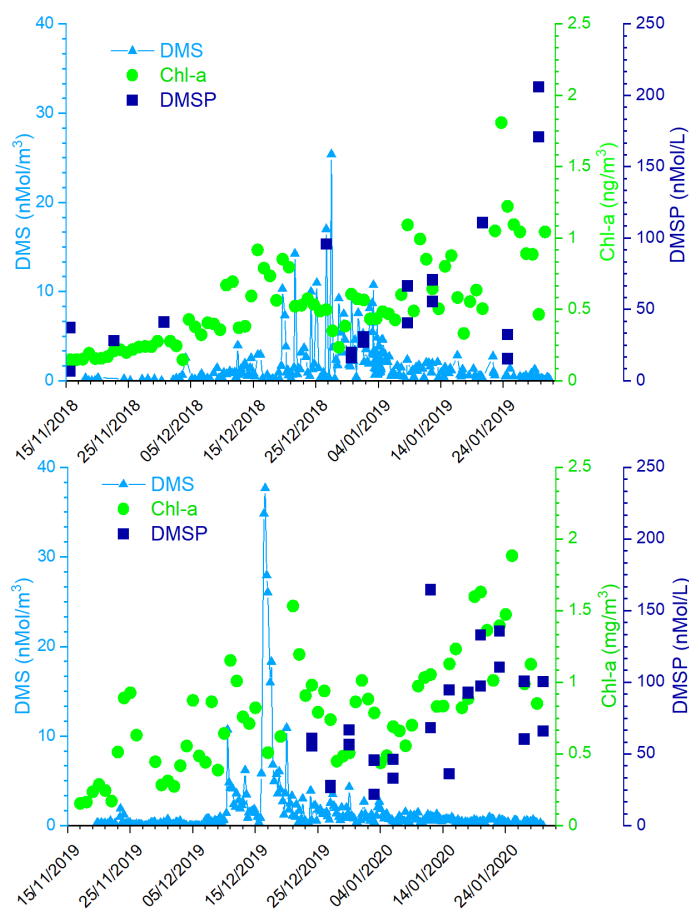
Therefore, the DMS concentration in the atmosphere does not seem to be controlled by physical processes at the ocean/atmosphere interface but is likely related to biological processes in the ocean.

295 Previous studies found that DMS concentrations in seawater are related to phytoplanktonic biomass (expressed by Chl-a concentration) or to primary productivity, that are in turn controlling the biogenic aerosol (Minikin et al., 1998; Preunkert et al., 2007).

Some of the highest DMS concentrations in seawater worldwide (>300 nMol/L) have been reported from the Ross Sea, Antarctica, associated with seasonal blooms of the phytoplankton *Phaeocystis a.* (Ditullio et al., 2003; Gambaro et al., 2004), a high-DMSP producer (Liss et al., 1994).

300 Fig. 3 shows the time series of measured atmospheric DMS and marine DMSP concentrations, and of satellite-derived Chl-a in the two ACs. The satellite determinations of Chl-a are averaged over the region 162.5977°E, 77.666°S; 171.2109°E,

72.2168°S, which corresponds to the area of a rectangle 600x300 km covering the polynya area facing MZS. Evidently, the first maxima in Chl-a are followed by increased DMS values in the atmosphere. Also, the first Chl-a double-peak in late November early December 2019 is higher (1.2-1.8 mg/m³) than the first peak in mid-December of 2018 (0.9 mg/m³). A similar pattern is visible in DMS concentration, with a higher peak in early December 2019 (921 pptV = 37.7 nMol/m³) than in late December 2018 (620 pptV = 25.4 nMol/m³). This seasonal DMS accumulation may be caused by a combination of factors, including high DMS production rates, limitation of bacterial DMS consumption at low temperatures, and saturation of biological DMS consumption rates (Ditullio et al., 2003; del Valle et al., 2009).



310

Figure 3. Time series of measured atmospheric DMS, DMSP in sea water, and satellite-derived Chl-a (daily, area averaged concentration in the region 162.5977°E, 77.666°S; 171.2109°E, 72.2168°S, corresponding to a rectangle 600 x 300km) in the two ACs.

315 Particularly relevant is the time lag of about 15 days in both Antarctic campaigns between the Chl-a and the DMS peaks. This delay is expected because DMS emissions depend on the physiological state of the phytoplankton. In particular, large emissions are connected with the phytoplanktonic senescent phase associated with stress factors, such as increasing solar radiation due to the shallowing of the depth of the mixing layer (Simó et al., 1999; Vallina and Simó, 2007), consumption of nutrients (Sunda et al., 2007; Zindler et al., 2014), grazing (Savoca and Nevitt, 2014), and bacterial decomposition (Kiene and
320 Bates, 1990; Lomans et al., 2002). The senescent phase, and the DMS emission, generally follows the maximum of phytoplankton biomass coincident with the peak of Chl-a concentration.

It is interesting to note the presence in both the ACs of a second Chl-a peak in January. The Chl-a concentration peak in January is higher than the one in December, and it is not associated with an increase in DMS concentrations into the atmosphere (cf. Fig. 3), despite the high concentration of DMSP in surface seawater. To understand this mechanism DMS concentration
325 is sea water would have been useful, but as we do not have these measurements, we can speculate that DMS concentration in the surface ocean at any given time reflects a complex balance between its biological source, bacterial consumption, photochemical oxidation and ventilation to the atmosphere. Regarding the biological source the difference in community composition, which is dominated by *Phaeocystis a.* in early summer (November-December) when sea ice melts, and later by diatoms (Bolinezi et al., 2020; Innamorati et al., 2000) can affect the DMS concentration in sea water in early and late summer.
330 Indeed, it has been shown that in the Ross Sea the DMS:chl-a ratio (58–78 nMol/μg) was significantly higher in waters dominated by *P. antarctica* compared to diatom-dominated waters (2–12 nMol/μg) (DiTullio and Smith, 1995). Regarding the effect of biological DMS consumption, Del Valle et al.(2009) found that while it remained relatively low and constant throughout the spring (0.05–0.21 d⁻¹), it becomes higher in summer (0.22–0.98 d⁻¹; i.e., faster biological turnover). The spring slow biological turnover probably contributed to the DMS buildup during the early bloom, while the fast biological turnover
335 (leading to the formation of DMSO) helped in producing low DMS concentrations in summer (3.2–16.8 nMol/L). The higher biological DMS consumption in January than in December can explain the apparent anomaly of the higher concentration of DMSP in near surface sea water and low DMS in the atmosphere. Unfortunately, we could not collect sea water samples during the period of maximum atmospheric DMS concentration due to lack of safe conditions which prevented to reach the open sea. In addition to the different levels of Chl-a and DMS during the two Antarctic campaigns, the Chl-a peaks occurred with a
340 different timing. In particular, in summer 2018-19 Chl-a peak occurs later than in the 2019-2020 summer.

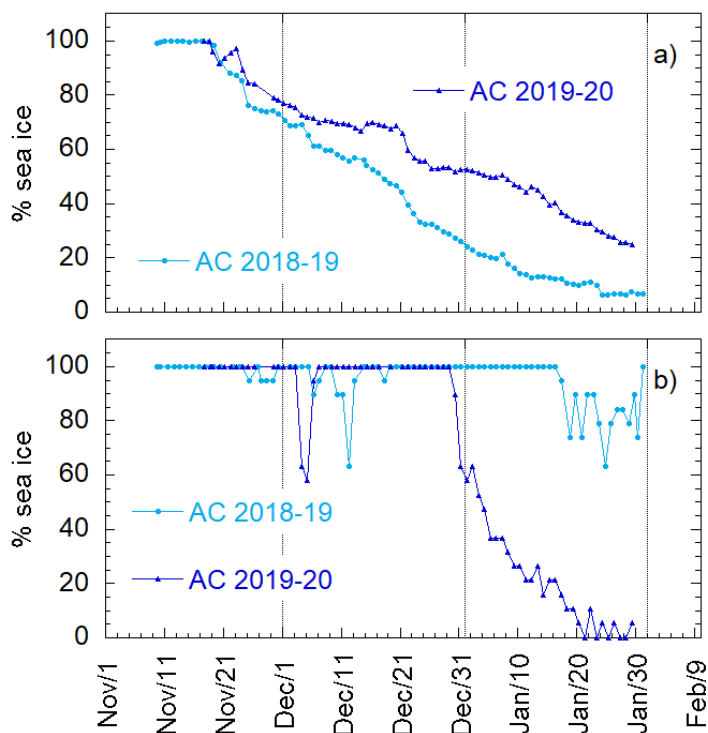


Figure 4. Percentage of the area covered by sea ice for the (a) Ross Sea (800x800 km²) and (b) the restricted area of polynya in the Ross Sea (100x100 km²) for the two ACs.

345

It is well known that phytoplanktonic blooms of *Phaeocystis a.* occur at the beginning of sea ice melting (Arrigo et al., 1998; Stefels et al., 2018). Fig. 4 shows the sea ice coverage, as determined by satellite observations, in two areas of the Ross Sea, for 2018-19 and 2019-20. When the whole Ross Sea area is considered (an area about 800x800 km²), it appears that the ice cover is higher in 2019-20 than in 2018-19, which seems in contrast to the timing of Chl-a increases. However, analyzing in detail the area of the polynya facing the sampling site (about 100x100 km² wide), we may observe that sea ice starts melting earlier and decreases faster in 2019-20 than the previous year. This evolution of sea ice in the region surrounding MZS could produce a shorter but more intense phytoplanktonic bloom in the polynya area in 2019-2020, and seems to be consistent with the observed evolution of DMS and related parameters. This suggests that the polynya areas close to MZS play a dominant role for the phytoplanktonic cycle and production of biogenic aerosol precursors.

355

3.2 The relationship between DMS and its oxidation products (MSA and nssSO₄²⁻): a schematic representation of mechanisms

The simultaneous measurements of atmospheric DMS and its oxidation products allow to study the dynamic processes occurring in the atmosphere leading to the formation of biogenic particulate matter. These processes can be summarized by the simple model reported in Fig. 5, where the box represent the atmosphere over the sampling site (and relative concentration of DMS, MSA and nssSO_4^{2-}). F_{DMS} , F_{MSA} , and $F_{\text{nssSO}_4^{2-}}$ are the flux of DMS, MSA and nssSO_4^{2-} incoming (F-in), outgoing (F-out) or formation (Fox). DMS_{sw} and DMS_{LR} represent the concentration of DMS in sea water and from sea water far from the sampling site (long range) respectively. MSA_{LR} and $\text{nssSO}_4^{2-}\text{LR}$ represent the concentration of long range transported species and $\text{nssSO}_4^{2-}\text{volc.}$ represent the volcanic nssSO_4^{2-} .

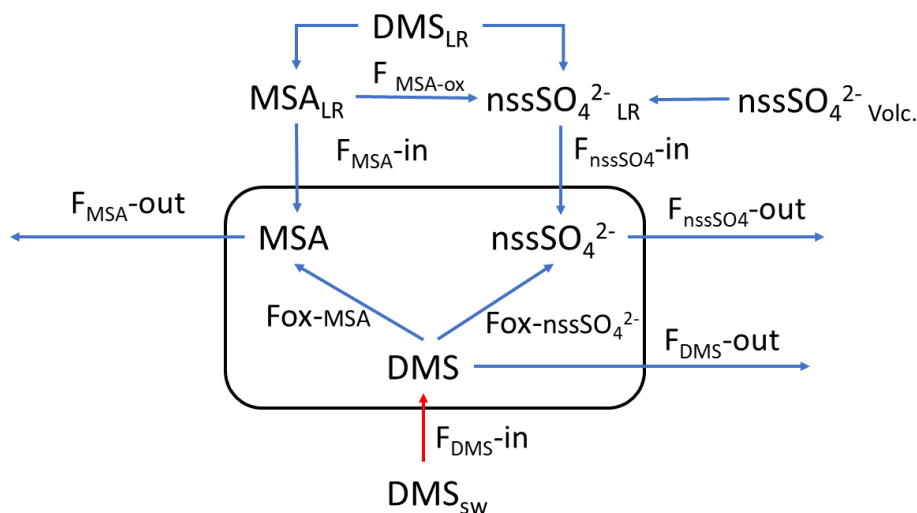


Figure 5. Schematic representation of the processes related to the measured concentration of DMS, MSA and nssSO_4^{2-} at MZS. See text for the abbreviations meaning.

370

In this section we discuss the overall evolution of DMS, MSA and nssSO_4^{2-} and their relationships, with the aim of identifying periods for which occurring processes, with respect to the DMS oxidation pathways, can be determined. Specific periods in which near/far sources of the different compounds and oxidation processes for different DMS emission conditions, are identified and discussed as explanatory cases.

375 Fig. 2 shows that in both ACs MSA displays a time evolution similar to nssSO_4^{2-} , with simultaneous peaks. Conversely, the time evolution of MSA and nssSO_4^{2-} differs from that of DMS in the two ACs: (i) during the 2019-2020 AC, maxima of biogenic aerosol compounds occur with a short time difference (24 h) with respect to the DMS peaks, (ii) during the 2018-2019 AC, the largest MSA and nssSO_4^{2-} peak occurs one month later than DMS.

In the period 15-18 December 2019 (Fig. 6) MSA and nssSO_4^{2-} maxima are associated with DMS. This case offers an exceptional example to understand the dynamics of biogenic aerosol formation. In this period air masses arrived from the area of the Ross Sea surrounding the sampling site (Fig. 7a) passing at low height on the near sea areas not covered by sea ice,

380

therefore in correspondence with strong DMS emission from sea water. The wind speed and direction are almost constant at about 10 m/sec from the marine sector (180-220°N). The measured relative humidity is 100%, and UV radiation is attenuated by clouds until 17 December at 00:00 (Fig. 6). Looking at the scheme in Fig. 5, from 16 to 17 December 2019 we assumed that $F_{\text{DMS-in}}$ is constant and quite high; at the beginning of DMS emission (16 December 2019) $F_{\text{ox-MSA}}$ and $F_{\text{ox-nssSO}_4}$ just started therefore the concentration of DMS in the box depend by the equilibrium between $F_{\text{DMS-in}}$ and $F_{\text{DMS-out}}$. At this wind speed $F_{\text{DMS-out}}$ is probably low respect to $F_{\text{DMS-in}}$ as the concentration DMS_{sw} (driving the sea-air flux) is high. In these conditions, the DMS concentration reached a maximum of 32.8 nMol/m³ on 16 December (average over the period 9:00-21:00 LT). Due to the constant wind speed and direction (Fig. 6) we can assume that DMS emission from the ocean remains constant also in the following days ($\text{DMS}_{\text{emitted}}$), when UV radiation increase in the following 24 h stimulated the DMS oxidation processes, $F_{\text{ox-MSA}}$ and $F_{\text{ox-nssSO}_4}$ become relevant and at constant $F_{\text{DMS-in}}$ and $F_{\text{DMS-out}}$, the concentration of MSA and nssSO_4^{2-} increases and DMS decreases. MSA and nssSO_4^{2-} reached the maximum concentration on December 17 (8.3 and 9.9 nMol/m³ for MSA and nssSO_4^{2-} , respectively, for the sampling time 9:00-21:00 LT), when the DMS concentration was 12.6 nMol/m³.

Therefore, the December 17 in the box of Fig. 5 we should have:

$$\text{DMS}_{\text{emitted}} = \text{DMS}_{\text{lost}} + \text{DMS}$$

$$\text{If } \text{DMS}_{\text{emitted}} = 32.8 \text{ nMol/m}^3 \text{ and DMS in the box is } 12.6 \text{ nMol/m}^3$$

$$\text{DMS}_{\text{lost}} = 32.8 - 12.6 = 20.2 \text{ nMol/m}^3$$

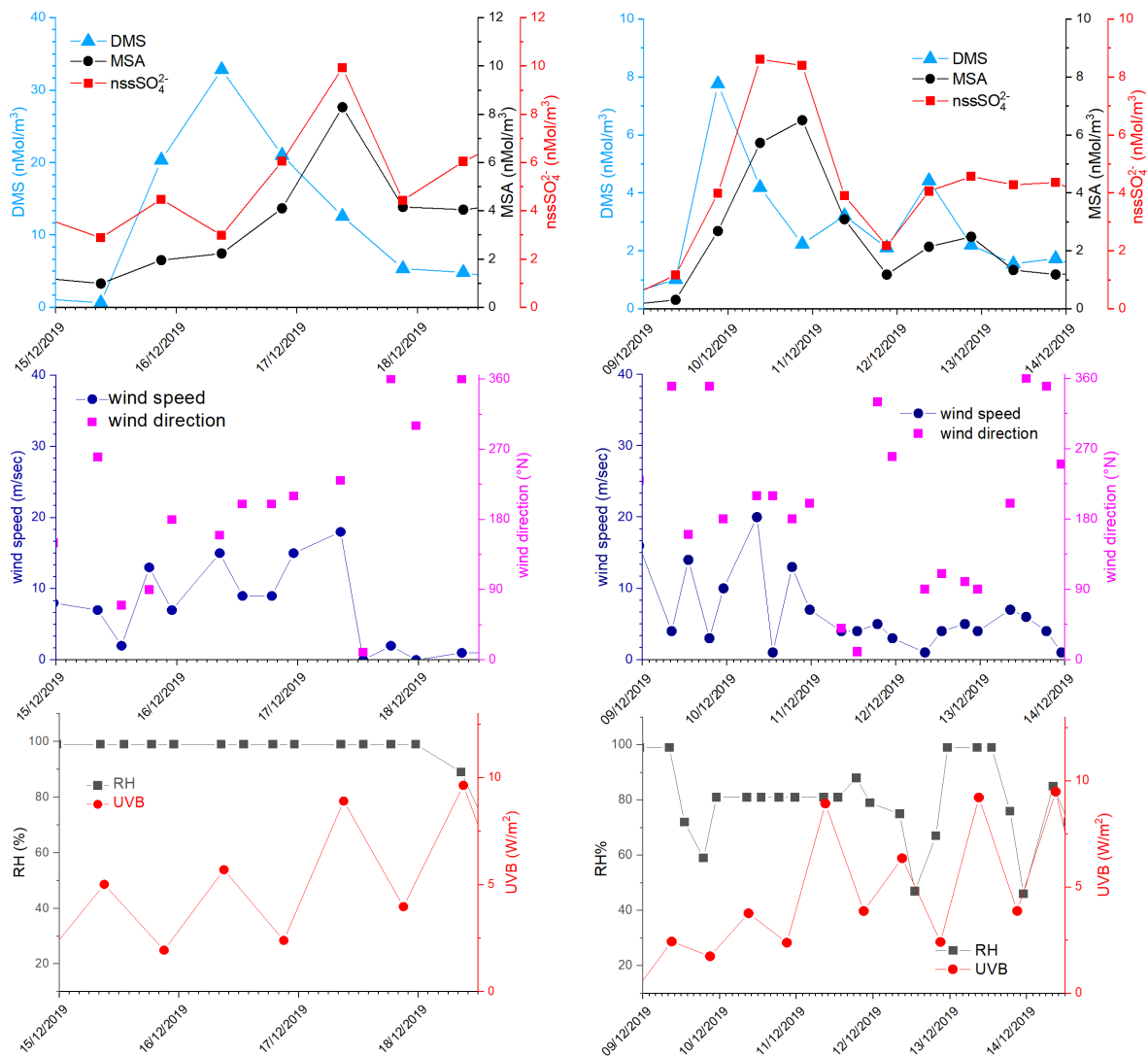
But the DMS_{lost} is due to the formation of MSA and nssSO_4^{2-} therefore:

$$\text{DMS}_{\text{lost}} = \text{MSA} + \text{nssSO}_4^{2-} = 8.3 + 9.9 = 18.2 \text{ nMol/m}^3 \text{ that is in agree with the value of } 20.2 \text{ previously calculated with the approximation of the constant DMS emission in these days.}$$

Therefore, in this situation of constant wind speed and direction the 17 December we can suppose that F_{MSA} and $F_{\text{nssSO}_4^{2-}}$ in and out are negligible and the concentration of MSA and nssSO_4^{2-} in the box are mainly due to the $F_{\text{ox-MSA}}$ and $F_{\text{ox-nssSO}_4^{2-}}$, for this reason reflecting the MSA/ nssSO_4^{2-} ratio of freshly formed biogenic aerosol.

In the following day (18 December) the abrupt change of wind direction (Figure 5) transport on the sampling site different air masses, therefore progressively increasing $F_{\text{DMS-out}}$, $F_{\text{MSA-out}}$ $F_{\text{nssSO}_4^{2-}-out}$ leading to MSA, nssSO_4^{2-} and DMS concentration decreases in the box of Fig. 5.

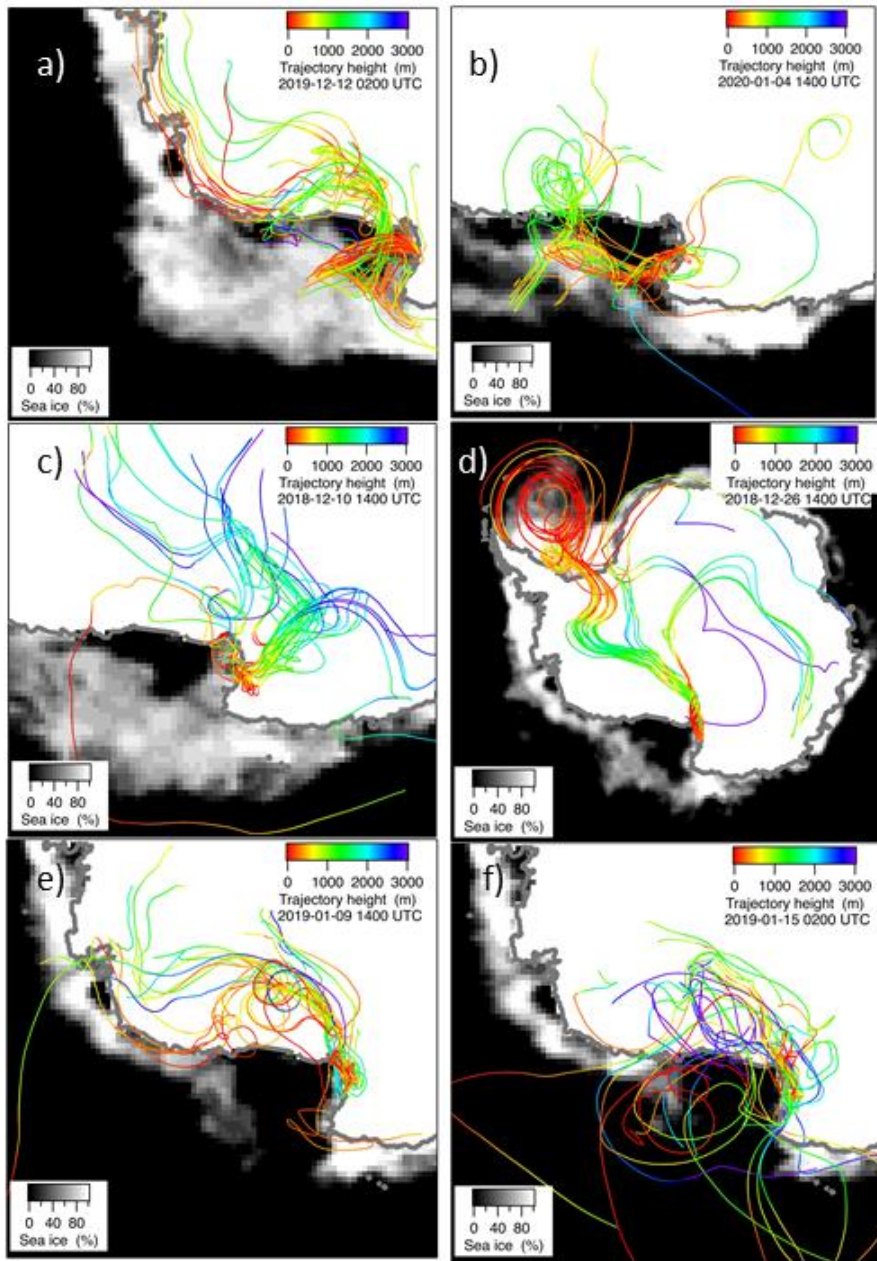
In the days 16-17 December, the MSA/ nssSO_4^{2-} ratio ranges from 0.68 to 0.94 mol/mol. As reported by Fung et al. (2022) the BrO reaction with DMS in gas phase and O₃ reaction in aqueous phase are the two main processes for DMS loss in southern high latitude ocean accounting for 50-60% and 20-30 % respectively. Both these processes lead to the formation of MSA in aerosol phase (Fung et al., 2022). In particular, the reaction with O₃ in aqueous phase could be particularly efficient at this time when high relative humidity is measured (100%). This high MSA/ nssSO_4^{2-} ratio can be measured only in the freshly formed secondary biogenic aerosol as MSA in aerosol phase can be transformed in nssSO_4^{2-} by reaction with OH radicals (Fung et al., 2022) leading to a decrease of the MSA/ nssSO_4^{2-} ratio in the aged aerosol.



415

Figure 6. DMS, MSA and nssSO₄²⁻, wind speed and direction, relative humidity (RH) and UVB for the time 15-19 December 2019 and 9-14 December 2019. DMS and UV-B data are averaged over the time interval of the corresponding aerosol sampling (12h).

420

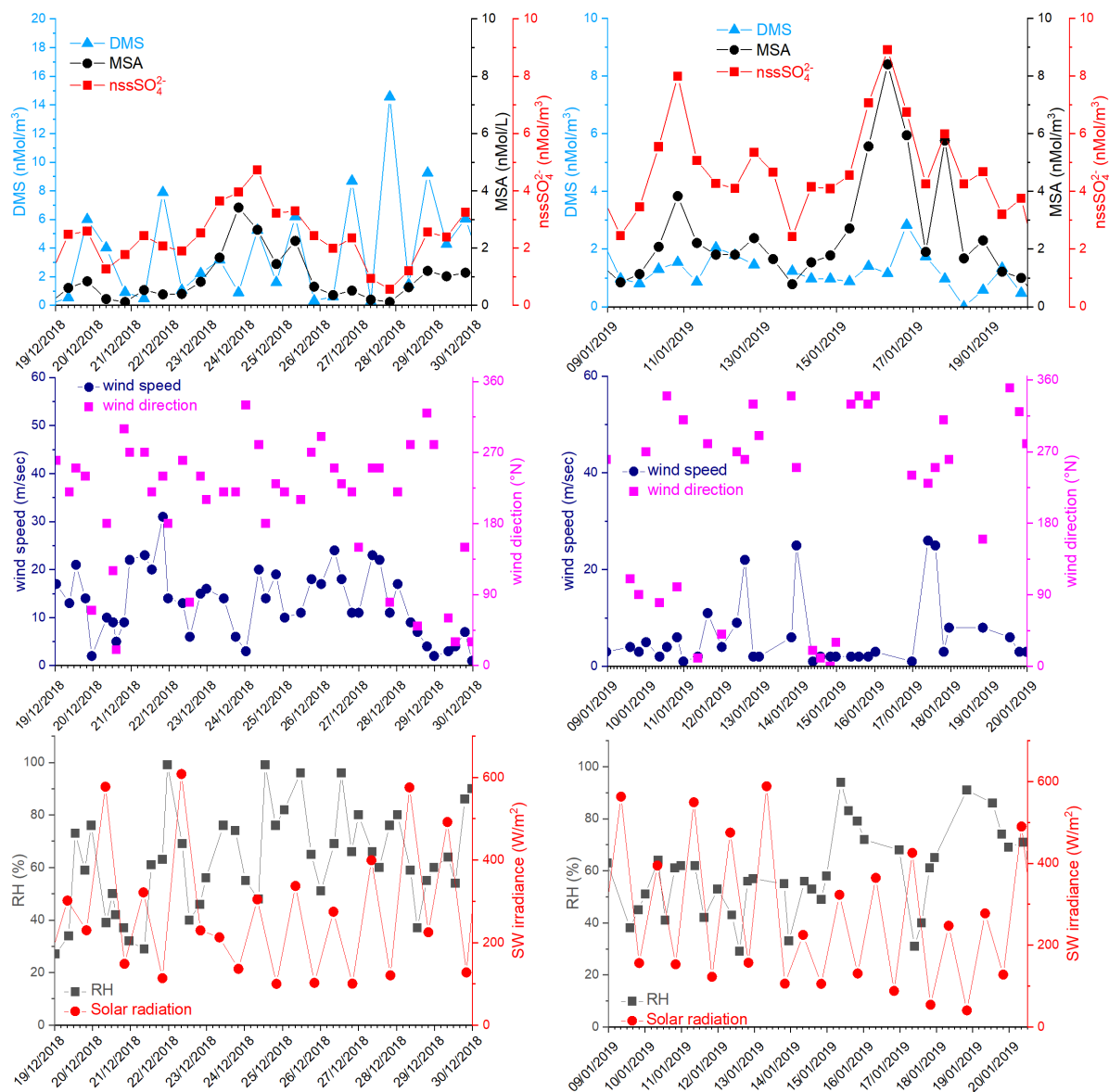


425 **Figure 7. Ensemble of ten-day backward trajectories at 300 m a.g.l. arrival height for the days 16 December 2019 (a), 4 January 2020 (b), 10 December 2018(c), 26 December 2018 (d), 9 January 2019 (e), 15 January 2019 (f) together with the ice cover for these days. Trajectory height along the route and sea ice percentage are presented as color or gray scales respectively.**

A similar situation occurred also in the period 9-15 December, 2019, and 3-7 January, 2020 (the latter reported as an example in Fig. 6, and the corresponding backward trajectories in Fig. 7b) even though with different intensity of DMS emissions. In the 2018-2019 AC, conversely, MSA and nssSO_4^{2-} maxima do not strictly coincide with high DMS concentrations. In particular:

1. The first peaks of MSA and nssSO_4^{2-} occur on 10-11 December, 2018, about 10 days before the main DMS peak. Sea ice is still present near the sampling site and DMS can not escape locally to the atmosphere, therefore $F_{\text{DMS-in}}$ (cfr. Fig 5) is low, therefore is low also the concentration of DMS in the box. At this time MSA and nssSO_4^{2-} were very likely transported from areas far from the sampling site (i.e. MSA_{LR} and $\text{nssSO}_4^{2-\text{LR}}$ -Fig.5) where an early phytoplankton bloom was taking place likely due to the sea ice melting in the external boundary of sea ice belt around Antarctica (Gabric et al., 2005; Gabric et al., 2018). Backward trajectories show air masses coming from the ice sheet (cf. Fig. 7c); therefore, we can suppose that MSA and nssSO_4^{2-} came from oceanic sectors far from the sampling site. In this period, the MSA/ nssSO_4^{2-} ratio was quite low (about 0.2), indicating generally aged air masses.
2. In the period 19-30 December, 2018, several DMS peaks were measured, associated with low or moderate MSA and nssSO_4^{2-} concentrations (Fig.8). In this period DMS emissions from the ocean are expected to be high and to be captured by the air masses traveling over the sea. This period is characterized by high wind speeds; DMS concentration spikes are higher when wind speed drops (Fig. 8). In this case due to high variability of wind speed with values up to 25-30 m/sec $F_{\text{DMS-in}}$ (Fig.5) can be high, but in this condition is also high $F_{\text{DMS-out}}$ (Fig.5) therefore the DMS laden air masses are transported away before a relevant amount of product (MSA and nssSO_4^{2-}) are formed. Therefore, even if a small amount of measured MSA and nssSO_4^{2-} in the box can come from $F_{\text{ox-MSA}}$ and $F_{\text{ox-nssSO}_4}$, the main part come from $F_{\text{MSA-LR}}$ and $F_{\text{nssSO}_4\text{-LR}}$. As $\text{nssSO}_4^{2-\text{LR}}$ can arise from the further oxidation of MSA in water phase along the transport ($F_{\text{MSA-ox}}$, Fung et al., 2022) and from volcanic sources ($\text{nssSO}_4^{2-\text{volc.}}$) the measured MSA/ nssSO_4^{2-} ratio is lower and more variable respect to those measured in freshly formed biogenic aerosol. The backward trajectories show that airmasses came from the Weddel Sea, far from the sampling site (Fig. 7d), crossing the ice sheet and passing at low elevation over the Terra Nova Bay polynya just before arriving to the sampling site. The presence of generally aged air masses in this period is confirmed by the low MSA/ nssSO_4^{2-} ratio (0.35 on average). Therefore, in these periods airmasses containing MSA and nssSO_4^{2-} came from an oceanic sector far from the sampling site, whereas the DMS enters the air mass over the polynya just before the sampling site.
3. In the two periods 9-13, and 15-18 January, 2019, high MSA and nssSO_4^{2-} concentrations ($> 5 \text{ nMol/m}^3$) are measured, while DMS concentrations are very low ($< 3 \text{ nMol/m}^3$). In these periods wind speed was very low ($< 5 \text{ m/sec}$) (Fig. 8). Backward trajectories show air masses coming from the ice sheet for the period 9-13 January (Fig. 7e) and routes extremely variable sometimes coming from the northern part of Ross Sea uncovered by ice at this time. (Fig. 7f). Indeed, the MSA/ nssSO_4^{2-} ratio, is quite low on 9-13 January (0.40 Mol/Mol) when air masses come from ice sheet and therefore far from the sampling site, while it reaches the highest measured value (up to 0.96 Mol/Mol) during 15-

18 January suggesting the presence of freshly formed biogenic aerosol from DMS formed in the northernly in the Ross Sea.



465 **Figure 8.** DMS, MSA and nssSO₄²⁻, wind speed and direction, relative humidity (RH) and short-wave irradiance for the time 19-30th December 2018 and 9-20th January 2019. DMS and SW irradiance data are averaged over the same time interval of the aerosol sampling (12h).

3.3 Quantification of the biogenic aerosol contribution to PM₁₀

470

In the previous section we highlighted the variability of the MSA/nssSO₄²⁻ ratio as a function of the air masses aging. In order to find a characteristic branch ratio for the DMS oxidation, the MSA concentrations are reported versus nssSO₄²⁻ concentrations in Fig. 9. A somewhat different pattern of MSA concentration with respect to nssSO₄²⁻ concentrations appears. We separated data into two classes, respectively for nssSO₄²⁻ values lower and higher than the somewhat arbitrary value of 3 nMol/m³. The slope of the MSA-nssSO₄²⁻ relationship appears to change approximately around this value. Small changes in the results that will be discussed occur when a different threshold value in the range 2.5-4 nMol/m³ is chosen.

475

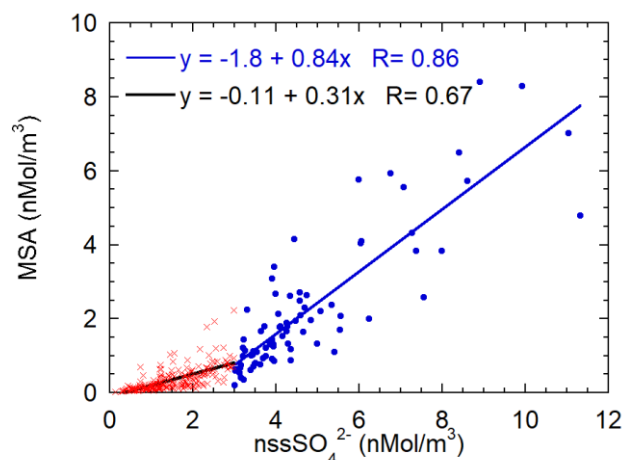


Figure 9. Scatter plot of MSA concentrations versus nssSO₄²⁻. The two regression lines are calculated for nssSO₄²⁻ concentration lower (red crosses, black line) and higher (blue dots and line) than 3 nMol/m³.

480

The value of the threshold allows to split the data set in low and high biogenic aerosol load. The presence or high or low biogenic aerosol load is related both to the air masses direction and timing. About the 60% of data with nssSO₄²⁻ concentration lower than 3 nMol/m³ comes from the ice sheet (direction from 200-350°N as above reported), the remaining 40% are related to a time before the beginning of sea ice melt and therefore before the phytoplanktonic bloom.

485

MSA shows a relatively high correlation with nssSO₄²⁻ for both data set (even though the correlation is worse for low nssSO₄²⁻ concentrations) suggesting that both species have a common source, as expected for DMS oxidation. The slope of the regression line is higher for the class with nssSO₄²⁻ > 3 nMol/m³. The two different slopes can be associated with different situations: for nssSO₄²⁻-concentrations below 3 nMol/m³, the MSA-nssSO₄²⁻ relationship is expected to be produced by aged biogenic aerosol, with possible additional nssSO₄²⁻ contributions coming from the oxidation of SO₂ emitted by the near volcano

490

Erebus (Boichu et al., 2015)(Fig. 1), or from long range transport from northern latitudes (Minikin et al., 1998).

Conversely, nssSO_4^{2-} values higher than 3 nMol/m^3 appear to be generally associated with the presence of freshly formed biogenic aerosol. The abscissa-intercept of the regression line is 2.1 nMol/m^3 , corresponding to 202 ng/m^3 . Once this background contribution is subtracted, the MSA/nssSO_4^{2-} derived from the regression line is $0.84 \pm 0.06 \text{ Mol/Mol}$ (that is the same value expressed as w/w as MSA and SO_4^{2-} have almost the same molar mass). We assume that this value can be considered as the mean branch ratio between the two species in the newly formed biogenic aerosol in summer at this high southern latitude. Several other studies report quite different MSA/nssSO_4^{2-} ratios, both in aerosol and snow layers (Becagli et al., 2005; Legrand and Pasteur, 1998; Minikin et al., 1998; Mulvaney and Wolff, 1994; Preunkert et al., 2008; Zhang et al., 2015). However, some of these determinations are affected by fractionation effects in the aerosol during the transport from source regions to the sampling site, and by different deposition processes. In this study, thanks to the closeness and strength of the DMS source during periods of ice-free polynya in the short range of the sampling site, and to the opportunity to find air masses containing DMS and both its freshly formed oxidation products, we believe that it is possible to obtain a characteristic MSA/nssSO_4^{2-} branch ratio for the freshly formed biogenic sulfur oxidized aerosol.

Considering the samples when nssSO_4^{2-} is higher than 3 nMol/m^3 as representative of the presence of freshly formed biogenic aerosol, is it thus possible to quantify the role played by newly formed biogenic aerosol on the total PM_{10} mass. On average, the sum of biogenic nssSO_4^{2-} (i.e. by subtracting the nssSO_4^{2-} -background) and MSA accounts for 17% of the PM_{10} mass, with maxima in single samples as high as 56%. This contribution is relevant, and its quantification is important also from a climatic point of view, as freshly formed biogenic aerosol can constitute an important source of cloud condensation nuclei over the Southern Ocean.

510 **4. Summary and conclusions**

Simultaneous high time resolution measurements of sulfur-compounds have been collected at a coastal Antarctic site (MZS) during two summer campaigns (2018-2019 and 2019-2020), to provide information on marine biological activity in the nearby polynya in the Ross Sea and on the influence of biogenic and atmospheric processes on biogenic aerosol formation.

Data on atmospheric DMS concentration are scarce especially in Antarctica. The DMS-maximum at MZS occurs in December, one month earlier than at the other sites at lower southern latitudes where measurements are available. The maximum of DMS concentration appears to be connected with the phytoplanktonic senescent phase following the bloom of *P. antarctica* that occurs in the polynya area closest to the sampling site, when sea ice opens up.

The second plankton bloom is related to diatoms and occurs in January. During this bloom, despite the high DMSP concentration in sea water, atmospheric DMS remained low probably due to its fast biological turnover in sea water in this period (Del Valle et al., 2009). DMS measurements in sea water may help elucidate the connection between Chl-a, DMSP in the ocean and DMS into the atmosphere.

The intensity and timing of the DMS evolution during the two years also suggests that only the portion of the polynya close to the sampling site produces a discernible effect on the measured DMS.

Several studies highlight the necessity to determine the branch ratio between MSA and nssSO_4^{2-} from DMS oxidation at high latitudes. However, the DMS oxidation responds to multiple processes and controllers, including concentration of atmospheric oxidants and meteorological factors; therefore, the values of the branch ratio found in the literature vary considerably (e.g., Bates et al., 1992, Preunkert et al., 2008; Yan et al., 2020). In this study, the closeness to the DMS source area, and the occurrence of air masses containing DMS and freshly formed oxidation products allow a reliable derivation of the branch ratio. The MSA/ nssSO_4^{2-} branch ratio for newly formed biogenic aerosol is estimated to be 0.84 ± 0.06 .

Conversely, data suggest that for aged air masses with low DMS content, an enrichment of nssSO_4^{2-} with respect to MSA, due to the presence of background concentration of nssSO_4^{2-} from volcanic origin (Erebus) or coming from long range transport where part of MSA is converted in nssSO_4^{2-} in aqueous phase by radical OH. Therefore, the aged air mass presents MSA/ nssSO_4^{2-} ratio lower than in newly formed biogenic aerosol.

By considering the sum of MSA and biogenic nssSO_4^{2-} in periods impacted by fresh biogenic aerosol, we estimate that the mean contribution of biogenic particulate matter to PM_{10} is 17%, with a maximum of 56%. The high contribution of biogenic aerosol to the total PM_{10} mass in summer in this area highlights the dominant role of the polynya area on biogenic aerosol formation. This is especially important due to the possible relevant role played by this aerosol in CCN formation.

Finally, due to the regional and year-to-year variability of DMS and related biogenic aerosol formation, we stress the need for long-term DMS measurements both in sea water and into the atmosphere together with biogenic aerosol along the Antarctic coast and in the Southern Ocean. This is particularly important in this phase, in which increasing temperatures and fast changes of ice distribution and properties are expected to affect other environmental parameters, such as primary productivity, formation of biogenic aerosols, and consequent climate-related parameters.

Code/Data availability

Data are available on request to the corresponding authors.

Author contribution

S.B.: Conceptualization; Investigation; Writing. E.B., Methodology; Data curation. S.Bo.: Methodology; Data curation. LC: Methodology; Data curation. AdS: Conceptualization; Investigation. M.F: Methodology; Data curation. P.G.: Methodology; Data curation. J.H.: Conceptualization; Investigation. L.L.: Conceptualization; Investigation. M.L.: Investigation. A.M.: Methodology; Data curation. M.M. Methodology; Data curation. C.M.: Methodology; Data curation. D.M.: Conceptualization; Investigation. C.N.: Methodology; Data curation. G.P.: Methodology; Data curation. K.-T.P. Methodology; Data curation. S.P.: Investigation. M.S. Validation; Investigation. M.V.: Methodology; Data curation. R.Z.: Methodology; Data curation. R.T.: Validation; Investigation; Funding acquisition.

555

Declaration of interests

The authors declare that they have no known competing financial interests or personal relationships that could have appeared to influence the work reported in this paper.

560 **Acknowledgements**

The research was financially supported by the MIUR (Italian Ministry of University and Research) and PNRA (Programma Nazionale di Ricerca in Antartide) through the PNRA16_00065-A1 Project “Correlation between biogenic aerosol and primary production in the Ross Sea -BioAPRoS”.

565 Meteorological data are furnished by the “Meteo-Climatological Observatory at MZS and Victoria Land” project funded by the PNRA (PNRA14_00019) and managed by staff of the Italian National Agency for New Technologies, Energy and Sustainable Economic Development (ENEA) (www.climantartide.it)

We would like to thank the National Snow and Ice Data Center (NSIDC) funded through the NASA Earth Science Data and Information System (ESDIS) project and the Global Data Assimilation System (GDAS1) provided by the US National Weather Service's National Centers for Environmental Prediction (NCEP) for archiving and publishing the data.

570 Finally, a special thanks to the logistic and scientific staff at “Mario Zucchelli Station“ in the Antarctic campaigns 2018-19 and 2019-20, without them this work could not have been accomplished.

References

- Andreae, M. O. and Barnard, W. R.: The marine chemistry of dimethylsulfide, *Mar. Chem.*, 14(3), 267–279, doi:10.1016/0304-
575 4203(84)90047-1, 1984.
- Asher, E. C., Dacey, J. W. H., Stukel, M., Long, M. C. & Tortell, P. D.: Processes driving seasonal variability in DMS, DMSP, and DMSO concentrations and turnover in coastal Antarctic waters, *Limnol. Oceanogr.*, 62, 104–124; 2017.
- Ardyna, M., Claustre, H., Sallée, J. B., D’Ovidio, F., Gentili, B., van Dijken, G., D’Ortenzio, F. and Arrigo, K. R.: Delineating environmental control of phytoplankton biomass and phenology in the Southern Ocean, *Geophys. Res. Lett.*, 44(10), 5016–
580 5024, doi:10.1002/2016GL072428, 2017.
- Arrigo, K. R. and van Dijken, G. L.: Phytoplankton dynamics within 37 Antarctic coastal polynya systems, *J. Geophys. Res. Ocean.*, 108(C8), 3271, doi:10.1029/2002JC001739, 2003.
- Arrigo, K. R., Weiss, A. M. and Smith, W. O.: Physical forcing of phytoplankton dynamics in the southwestern Ross Sea, *J. Geophys. Res. Ocean.*, 103(C1), 1007–1021, doi:10.1029/97jc02326, 1998.
- 585 Arrigo, K. R., Lowry, K. E. and van Dijken, G. L.: Annual changes in sea ice and phytoplankton in polynyas of the Amundsen Sea, Antarctica, *Deep. Res. Part II Top. Stud. Oceanogr.*, 71–76, 5–15, doi:10.1016/j.dsr2.2012.03.006, 2012.
- Barnard, W. R., Andreae, M. O. and Iverson, R. L.: Dimethylsulfide and *Phaeocystis poucheti* in the southeastern Bering Sea, *Cont. Shelf Res.*, 3(2), 103–113, doi:10.1016/0278-4343(84)90001-3, 1984.

- 590 Becagli, S., Proposito, M., Benassai, S., Gragnani, R., Magand, O., Traversi, R. and Udisti, R.: Spatial distribution of biogenic sulphur compounds (MSA, nssSO₄²⁻) in the northern Victoria Land-Dome C-Wilkes Land area, East Antarctica, *Ann. Glaciol.*, 41, doi:10.3189/172756405781813384, 2005.
- Becagli, S., Marchese, C., Caiazzo, L., Ciardini, V., Lazzara, L., Mori, G., Nuccio, C., Scarchilli, C., Severi, M. and Traversi, R.: Biogenic aerosol in central East Antarctic Plateau as a proxy for the ocean-atmosphere interaction in the Southern Ocean, *Sci. Total Environ.*, 810, 151285, doi:10.1016/j.scitotenv.2021.151285, 2022.
- 595 Bell, T. G., Landwehr, S., Miller, S. D., de Bruyn, W. J., Callaghan, A. H., Scanlon, B., Ward, B., Yang, M., and Saltzman, E. S.: Estimation of bubble-mediated air–sea gas exchange from concurrent DMS and CO₂ transfer velocities at intermediate–high wind speeds, *Atmos. Chem. Phys.*, 17, 9019–9033, <https://doi.org/10.5194/acp-17-9019-2017>, 2017. Belviso, S., Moulin, C., Bopp, L. and Stefels, J.: Assessment of a global climatology of oceanic dimethylsulfide (DMS) concentrations based on SeaWiFS imagery (1998–2001), *Can. J. Fish. Aquat. Sci.*, 61(5), 804–816, doi:10.1139/F04-001, 2004.
- 600 Bock, J., Michou, M., Nabat, P., Abe, M., Mulcahy, J. P., Olivié, D. J. L., Schwinger, J., Suntharalingam, P., Tjiputra, J., van Hulten, M., Watanabe, M., Yool, A., and Séférian, R.: Evaluation of ocean dimethylsulfide concentration and emission in CMIP6 models, *Biogeosciences*, 18, 3823–3860, <https://doi.org/10.5194/bg-18-3823-2021>, 2021.
- Boden, R., Murrell, J. C. & Schäfer, H. Dimethylsulfide is an energy source for the heterotrophic marine bacterium *Sagittula stellata*. *FEMS Microbiol. Lett.* 322, 188–193, 2011.
- 605 Boichu, M., Oppenheimer, C., Tsanev, V., Kyle, P. R., Boichu, M., Oppenheimer, C., Tsanev, V. and Kyle, P. R.: High temporal resolution SO₂ flux measurements at Erebus volcano , Antarctica To cite this version : HAL Id : hal-01157827 High temporal resolution SO₂ flux measurements at Erebus volcano , Antarctica, 2015.
- Bolinesi, F., Saggiomo, M., Ardini, F., Castagno, P., Cordone, A., Fusco, G., Rivaro, P., Saggiomo, V. and Mangoni, O.: Spatial-Related Community Structure and Dynamics in Phytoplankton of the Ross Sea, Antarctica, *Front. Mar. Sci.*, 7(December), doi:10.3389/fmars.2020.574963, 2020.
- 610 Cameron-Smith, P., Elliott, S., Maltrud, M., Erickson, D. and Wingenter, O.: Changes in dimethyl sulfide oceanic distribution due to climate change, *Geophys. Res. Lett.*, 38(7), doi:10.1029/2011GL047069, 2011.
- Charlson, R. J., Lovelock, J. E. Andreae, M. O. and Warren, S. G.: Oceanic phytoplankton, atmospheric sulphur, cloud albedo and climate., *Nature*, 326, 655–661, 1987.
- 615 Cole, H. S., Henson, S., Martin, A. P. and Yool, A.: Basin-wide mechanisms for spring bloom initiation: how typical is the North Atlantic?, *ICES J. Mar. Sci.*, 72(6), 2029–2040, doi:10.1093/ICESJMS/FSU239, 2015.
- Criscitiello, A. S., Das, S. B., Evans, M. J., Frey, K. E., Conway, H., Joughin, I., Medley, B. and Steig, E. J.: Ice sheet record of recent sea-ice behavior and polynya variability in the Amundsen Sea, West Antarctica, *J. Geophys. Res. Ocean.*, 118(1), 118–130, doi:10.1029/2012JC008077, 2013.
- 620 Dall’Osto, M., Beddows, D. C. S., Tunved, P., Krejci, R., Ström, J., Hansson, H. C., Yoon, Y. J., Park, K. T., Becagli, S., Udisti, R., Onasch, T., Ódowd, C. D., Simó, R. and Harrison, R. M.: Arctic sea ice melt leads to atmospheric new particle formation, *Sci. Rep.*, 7(1), doi:10.1038/s41598-017-03328-1, 2017.

- Deng, X., Chen, J., Hansson, L. A., Zhao, X. and Xie, P.: Eco-chemical mechanisms govern phytoplankton emissions of dimethylsulfide in global surface waters, *Natl. Sci. Rev.*, 8(2), 4–11, doi:10.1093/nsr/nwaa140, 2021.
- 625 Ditullio, G. R., Jones, D. R., and Geesey, M. E.: Dimethylsulfide Dynamics in the Ross Sea During Austral Summer,” in *Biogeochemistry of the Ross Sea* (American Geophysical Union (AGU)), 279–293, 2003. DiTullio, G. R. and Smith, W. O.: Relationship between dimethylsulfide and phytoplankton pigment concentrations in the Ross Sea, Antarctica, *Deep. Res. Part I*, 42(6), 873–892, doi:10.1016/0967-0637(95)00051-7, 1995.
- 630 Ducklow, H. W., Baker, K., Martinson, D. G., Quetin, L. B., Ross, R. M., Smith, R. C., Stammerjohn, S. E., Vernet, M. and Fraser, W.: Marine pelagic ecosystems: The West Antarctic Peninsula, *Philos. Trans. R. Soc. B Biol. Sci.*, 362(1477), 67–94, doi:10.1098/rstb.2006.1955, 2007.
- Faloona, I.: Sulfur processing in the marine atmospheric boundary layer: A review and critical assessment of modeling uncertainties, *Atmos. Environ.*, 43(18), 2841–2854, doi:10.1016/J.ATMOENV.2009.02.043, 2009.
- 635 Froelich, P. N., Kaul, L. W., Byrd, J. T., Andreae, M. O., Roe, K. K., Froelich, P. N., Kaul, L. W., Byrd, J. T., Andreae, M. O. and Roe, K. K.: Arsenic, barium, germanium, tin, dimethylsulfide and nutrient biogeochemistry in Charlotte Harbor, Florida, a phosphorus-enriched estuary, *ECSS*, 20(3), 239–264, doi:10.1016/0272-7714(85)90041-1, 1985.
- Fung, K. M., Heald, C. L., Kroll, J. H., Wang, S., Jo, D. S., Gettelman, A., Lu, Z., Liu, X., Zaveri, R. A., Apel, E. C., Blake, D. R., Jimenez, J.-L., Campuzano-Jost, P., Veres, P. R., Bates, T. S., Shilling, J. E., and Zawadowicz, M.: Exploring dimethyl sulfide (DMS) oxidation and implications for global aerosol radiative forcing, *Atmos. Chem. Phys.*, 22, 1549–1573, 640 <https://doi.org/10.5194/acp-22-1549-2022>, 2022.
- Gabric, A. J., Qu, B., Matrai, P. and Hirst, A.: The simulated response of dimethylsulfide production in the Arctic Ocean to global warming, *Tellus B: Chem. Phys. Meteorol.*, 57(5), 391–403, doi:10.3402/tellusb.v57i5.16564, 2005.
- Gabric, A. J., Qu, B., Matrai, P. A., Murphy, C., Lu, H., Lin, D. R., Qian, F. and Zhao, M.: Investigating the coupling between phytoplankton biomass, aerosol optical depth and sea-ice cover in the Greenland Sea, *Dyn. Atmos. Ocean.*, 66, 94–109, 645 doi:10.1016/J.DYNATMOCE.2014.03.001, 2014.
- Gambaro, A., Moret, I., Piazza, R., Andreoli, C., Rin, E. D. A., Capodaglio, G., Barbante, C. and Cescon, P.: Temporal evolution of DMS and DMSP in Antarctic Coastal Sea water, *Int. J. Environ. Anal. Chem.*, 84(6–7), 401–412, doi:10.1080/03067310310001636983, 2004.
- Gondwe, M., Krol, M., Gieskes, W., Klaassen, W. and De Baar, H.: The contribution of ocean-leaving DMS to the global 650 atmospheric burdens of DMS, MSA, SO₂, and NSS-SO₄⁻, *Global Biogeochem. Cycles*, 17(2), 1056, doi:10.1029/2002GB001937, 2003.
- Henderson, P. and Henderson, G. M.: *Earth Science Data*, Cambridge Univ. Press, 277, 2009.
- Hezel, P. J., Alexander, B., Bitz, C. M., Steig, E. J., Holmes, C. D., Yang, X. and Sciare, J.: Modeled methanesulfonic acid (MSA) deposition in Antarctica and its relationship to sea ice, *J. Geophys. Res. Atmos.*, 116(23), 1–18, 655 doi:10.1029/2011JD016383, 2011.

- Hulswar, S., Simo, R., Galí, M., Bell, T., Lana, A., Inamdar, S., Halloran, P. R., Manville, G., and Mahajan, A. S.: Third Revision of the Global Surface Seawater Dimethyl Sulfide Climatology (DMS-Rev3), *Earth Syst. Sci. Data Discuss.*, 2021, 1-56, 10.5194/essd-2021-236, 2021.
- 660 Innamorati, M., Mori, G., Massi, L., Lazzara, L. and Nuccio, C.: Phytoplankton Biomass Related to Environmental Factors in the Ross Sea, *Ross Sea Ecol.*, 217–230, doi:10.1007/978-3-642-59607-0_18, 2000.
- Jang, E., Park, K. T., Yoon, Y. J., Kim, K., Gim, Y., Chung, H. Y., Lee, K., Choi, J., Park, J., Park, S. J., Koo, J. H., Fernandez, R. P. and Saiz-Lopez, A.: First-year sea ice leads to an increase in dimethyl sulfide-induced particle formation in the Antarctic Peninsula, *Sci. Total Environ.*, 803, 150002, doi:10.1016/J.SCITOTENV.2021.150002, 2022.
- 665 Jarníková, T., Tortell, P. D., Jarníková, T. and Tortell, P. D.: Towards a revised climatology of summertime dimethylsulfide concentrations and sea–air fluxes in the Southern Ocean, *Environ. Chem.*, 13(2), 364–378, doi:10.1071/EN14272, 2016.
- Jourdain, B. and Legrand, M.: Seasonal variations of atmospheric dimethylsulfide, dimethylsulfoxide, sulfur dioxide, methanesulfonate, and non-sea-salt sulfate aerosols at Dumont d’Urville (coastal Antarctica) (December 1998 to July 1999), *J. Geophys. Res. Atmos.*, 106(D13), 14391–14408, doi:10.1029/2000JD900841, 2001.
- 670 Kettle, A. J. and Andreae, M. O.: Flux of dimethylsulfide from the oceans: A comparison of updated data sets and flux models, *J. Geophys. Res. Atmos.*, 105(D22), 26793–26808, doi:10.1029/2000JD900252, 2000.
- Kiene, R. P. and Bates, T. S.: Biological removal of dimethyl sulphide from sea water, *Nature*, 345, 702–705, 1990.
- Klimont, Z., Smith, S. J. and Cofala, J.: The last decade of global anthropogenic sulfur dioxide: 2000-2011 emissions, *Environ. Res. Lett.*, 8(1), doi:10.1088/1748-9326/8/1/014003, 2013.
- 675 Kloster, S., Six K. D., Feichter J., Maier-Reimer E., Roeckner E., Wetzel P., Stier P., and Esch M.: Response of dimethylsulfide (DMS) in the ocean and atmosphere to global warming, *J. Geophys. Res.*, 112, G03005, doi:10.1029/2006JG000224, 2007.
- Kloster, S., Feichter, J., Maier-Reimer, E., Six, K. D., Stier, P. and Wetzel, P.: DMS cycle in the marine ocean-atmosphere system - A global model study, *Biogeosciences*, 3(1), 29–51, doi:10.5194/BG-3-29-2006, 2006.
- Leck, C., Larsson, U., Bågander, L. E., Johansson, S. and Hajdu, S.: Dimethyl sulfide in the Baltic Sea: Annual variability in relation to biological activity, *J. Geophys. Res. Ocean.*, 95(C3), 3353–3363, doi:10.1029/JC095IC03P03353, 1990.
- 680 Legrand, M. and Pasteur, E. C.: Methane sulfonic acid to non-sea-salt sulfate ratio in coastal Antarctic aerosol and surface snow, *J. Geophys. Res. Atmos.*, 103(3339), 10991–11006, doi:10.1029/98JD00929, 1998.
- Liss, P. S., Malin, G., Turner, S. M. and Holligan, P. M.: Dimethyl sulphide and Phaeocystis: A review, *J. Mar. Syst.*, 5(1), 41–53 [online] Available from: [https://doi.org/10.1016/0924-7963\(94\)90015-9](https://doi.org/10.1016/0924-7963(94)90015-9), 1994.
- Lomans, B. P., Van der Drift, C., Pol, A. and Op den Camp, H. J. M.: Microbial cycling of volatile organic sulfur compounds, 685 *Cell. Mol. Life Sci.*, 59(4), 575–588, doi:10.1007/s00018-002-8450-6, 2002.
- Marandino, C. A., De Bruyn, W. J., Miller, S. D., & Saltzman, E. S.: Eddy correlation measurements of the air/sea flux of dimethylsulfide over the North Pacific Ocean. *J. of Geophys. Res.*, 112, D03301. <https://doi.org/10.1029/2006JD007293>, 2007.

- 690 Minikin, A., Legrand, M., Hall, J., Wagenbach, D., Kleefeld, C., Wolff, E., Pasteur, E. C. and Ducroz, F.: Sulfur-containing species (sulfate and methanesulfonate) in coastal Antarctic aerosol and precipitation, *J. Geophys. Res. Atmos.*, 103(3339), 10975–10990, doi:10.1029/98JD00249, 1998.
- Montes-Hugo, M., Doney, S. C., Ducklow, H. W., Fraser, W., Martinson, D., Stammerjohn, S. E. and Schofield, O.: Recent changes in phytoplankton communities associated with rapid regional climate change along the western Antarctic Peninsula, *Science* 323(5920), 1470–1473, doi:10.1126/science.1164533. 2009.
- 695 Mulvaney, R. and Wolff, E. W.: Spatial variability of the major chemistry of the Antarctic ice sheet, *Ann. Glaciol.*, 20, 440–447, doi:10.3189/1994AOG20-1-440-447, 1994.
- Nightingale, P. D., Liss, P. S. and Schlosser, P.: Measurements of air-sea gas transfer during an open ocean algal bloom, *Geophys. Res. Lett.*, 27(14), 2117–2120, doi:10.1029/2000GL011541, 2000.
- Oliver, H., St-Laurent, P., Sherrell, R. M. and Yager, P. L.: Modeling Iron and Light Controls on the Summer Phaeocystis antarctica Bloom in the Amundsen Sea Polynya, *Global Biogeochem. Cycles*, 33(5), doi:10.1029/2018GB006168, 2020.
- 700 Park, K.-T., Lee, K., Shin, K., Jin Jeong, H. and Young Kim, K.: Improved Method for Minimizing Sulfur Loss in Analysis of Particulate Organic Sulfur, *Anal. Chem.*, 86, 1352–1356, doi:10.1021/ac403649m, 2014.
- Preunkert, S., Legrand, M., Jourdin, B., Moulin, C., Belviso, S., Kasamatsu, N., Fukuchi, M. and Hirawake, T.: Interannual variability of dimethylsulfide in air and seawater and its atmospheric oxidation by-products (methanesulfonate and sulfate) at Dumont d’Urville, coastal Antarctica (1999–2003), *J. Geophys. Res. Atmos.*, 112(6), 1–13, doi:10.1029/2006JD007585, 2007.
- 705 Preunkert, S., Jourdain, B., Legrand, M., Udisti, R., Becagli, S. and Cerri, O.: Seasonality of sulfur species (dimethyl sulfide, sulfate, and methanesulfonate) in Antarctica: Inland versus coastal regions, *J. Geophys. Res. Atmos.*, 113(15), doi:10.1029/2008JD009937, 2008.
- Qu, B., Gabric, A. J. and Jackson, R.: Contemporary variability in dimethylsulfide flux in the Barents Sea and simulated change under 4×CO₂ climate conditions, *J. Mar. Syst.*, 220(December 2020), doi:10.1016/j.jmarsys.2021.103573, 2021.
- 710 Quinn, P. K. and Bates, T. S.: The case against climate regulation via oceanic phytoplankton sulphur emissions, *Nature*, 480(7375), 51–56, doi:10.1038/nature10580, 2011.
- Read, K. A., Lewis, A. C., Bauguitte, S., Rankin, A. M., Salmon, R. A., Wolff, E. W., Saiz-Lopez, A., Bloss, W. J., Heard, D. E., Lee, J. D. and Plane, J. M. C.: DMS and MSA measurements in the Antarctic Boundary Layer: Impact of BrO on MSA production, *Atmos. Chem. Phys.*, 8(11), 2985–2997, doi:10.5194/acp-8-2985-2008, 2008.
- 715 Saba, G. K., Fraser, W. R., Saba, V. S., Iannuzzi, R. A., Coleman, K. E., Doney, S. C., Ducklow, H. W., Martinson, D. G., Miles, T. N., Patterson-Fraser, D. L., Stammerjohn, S. E., Steinberg, D. K. and Schofield, O. M.: Winter and spring controls on the summer food web of the coastal West Antarctic Peninsula, *Nat. Commun.* 2014 51, 5(1), 1–8, doi:10.1038/ncomms5318, 2014.
- 720 Di Sarra, A., Fua, D., Cacciani, M., Di Iorio, T., Disterhoft, P., Meloni, D., Monteleone, F., Piacentino, S. and Sferlazzo, D.: Determination of ultraviolet cosine-corrected irradiances and aerosol optical thickness by combined measurements with a

- Brewer spectrophotometer and a multifilter rotating shadowband radiometer, *Appl. Opt.* Vol. 47, Issue 33, pp. 6142-6150, 47(33), 6142–6150, doi:10.1364/AO.47.006142, 2008.
- 725 Savoca, M. S. and Nevitt, G. A.: Evidence that dimethyl sulfide facilitates a tritrophic mutualism between marine primary producers and top predators, *Proc. Natl. Acad. Sci.*, 111(11), 4157–4161, doi:10.1073/PNAS.1317120111, 2014.
- Sciare, J., Mihalopoulos, N. and Dentener, F. J.: Interannual variability of atmospheric dimethylsulfide in the southern Indian Ocean, *J. Geophys. Res. Atmos.*, 105(D21), 26369–26377, doi:10.1029/2000JD900236, 2000.
- 730 Sherrell, R. M., Lagerström, M. E., Forsch, K. O., Stammerjohn, S. E. and Yager, P. L.: Dynamics of dissolved iron and other bioactive trace metals (Mn, Ni, Cu, Zn) in the Amundsen Sea Polynya, Antarctica, *Elementa*, 3, 71, doi:10.12952/JOURNAL.ELEMENTA.000071/, 2015.
- Simó, R.: Production of atmospheric sulfur by oceanic plankton: Biogeochemical, ecological and evolutionary links, *Trends Ecol. Evol.*, 16(6), 287–294, doi:10.1016/S0169-5347(01)02152-8, 2001.
- Simó, R.: From cells to globe: approaching the dynamics of DMS (P) in the ocean at multiple scales. *Canadian Journal of Fisheries and Aquatic Sciences* 61.5, 673-684, doi: 10.1139/f04-030, 2004.
- 735 Simó, R. and Pedrós-Alió, C.: Short-term variability in the open ocean cycle of dimethylsulfide, *Global Biogeochem. Cycles*, 13(4), 1173–1181, doi:10.1029/1999GB900081, 1999.
- Simó, R., Pedrós-Alió, C. and Simó, R. & Pedrós-Alió, C.: Role of vertical mixing in controlling the oceanic production of dimethyl sulphide, *Nature*, 402(6760), 396–398, doi:10.1038/46516, 1999.
- 740 St-Laurent, P., Yager, P. L., Sherrell, R. M., Stammerjohn, S. E. and Dinniman, M. S.: Pathways and supply of dissolved iron in the Amundsen Sea (Antarctica), *J. Geophys. Res. Ocean.*, 122(9), 7135–7162, doi:10.1002/2017JC013162, 2017.
- Stefels, J.: Physiological aspects of the production and conversion of DMSP in marine algae and higher plants, *J. Sea Res.*, 43(3–4), 183–187, doi:10.1016/S1385-1101(00)00030-7, 2000.
- 745 Stefels, J., Van Leeuwe, M. A., Jones, E. M., Meredith, M. P., Venables, H. J., Webb, A. L. and Henley, S. F.: Impact of sea-ice melt on dimethyl sulfide (sulfoniopropionate) inventories in surface waters of Marguerite Bay, West Antarctic Peninsula, *Philos. Trans. R. Soc. A Math. Phys. Eng. Sci.*, 376(2122), doi:10.1098/rsta.2017.0169, 2018.
- Stein, A. F., Draxler, R. R., Rolph, G. D., Stunder, B. J. B., Cohen, M. D. and Ngan, F.: NOAA’s HYSPLIT Atmospheric Transport and Dispersion Modeling System, *Bull. Am. Meteorol. Soc.*, 96(12), 2059–2077, doi:10.1175/BAMS-D-14-00110.1, 2015.
- 750 Sunda, W. G., Hardison, R., Kiene, R. P., Bucciarelli, E. and Harada, H.: The effect of nitrogen limitation on cellular DMSP and DMS release in marine phytoplankton: Climate feedback implications, in *Aquatic Sciences*, vol. 69, pp. 341–351., 2007.
- Tortell, P. D., Long, M. C., Payne, C. D., Alderkamp, A. C., Dutrieux, P. and Arrigo, K. R.: Spatial distribution of pCO₂, ΔO₂/Ar and dimethylsulfide (DMS) in polynya waters and the sea ice zone of the Amundsen Sea, Antarctica, *Deep. Res. Part II Top. Stud. Oceanogr.*, 71–76, 77–93, doi:10.1016/j.dsr2.2012.03.010, 2012.

- Trisolino, P., Di Sarra, A., Meloni, D., Pace, G., Anello, F., Becagli, S., Monteleone, F. and Sferlazzo, D.: Determination of Photosynthetically Active Radiation from multi-filter rotating shadowband measurements: Method and validation based on observations at Lampedusa (35.5°N, 12.6°E), in AIP Conference Proceedings, vol. 1810., 2017.
- 755 del Valle, D. A., Kieber, D. J., Toole, D. A., Bisgrove, J. and Kiene, R. P.: Dissolved DMSO production via biological and photochemical oxidation of dissolved DMS in the Ross Sea, Antarctica, *Deep. Res. Part I*, 2(56), 166–177, doi:10.1016/J.DSR.2008.09.005, 2009.
- 760 Del Valle, D. A., Kieber, D. J., Toole, D. A., Brinkley, J. and Kiene, R. P.: Biological consumption of dimethylsulfide (DMS) and its importance in DMS dynamics in the Ross Sea, Antarctica, *Limnol. Oceanogr.*, 54(3), 785–798, doi:10.4319/lo.2009.54.3.0785, 2009.
- Vallina, S. M. and Simó, R.: Strong relationship between DMS and the solar radiation dose over the global surface ocean, *Science*, 315(5811), 506–508, doi:10.1126/SCIENCE.1133680, 2007.
- 765 Vlahos, P. and Monahan, E. C.: A generalized model for the air-sea transfer of dimethyl sulfide at high wind speeds, *Geophys. Res. Lett.*, 36(21), 1–6, doi:10.1029/2009GL040695, 2009.
- Watanabe, S., Yamamoto, H. and Tsunogai, S.: Relation Between the Concentrations of DMS in Surface Seawater and Air in the Temperate North Pacific Region, Kluwer Academic Publishers., 1995.
- Wingenter, O. W., Haase, K. B., Zeigler, M., Blake, D. R., Rowland, F. S., Sive, B. C., Paulino, A., Thyraug, R., Larsen, A., 770 Schulz, K., Meyerhöfer, M. and Riebesell, U.: Unexpected consequences of increasing CO₂ and ocean acidity on marine production of DMS and CH₂Cl₂: Potential climate impacts, *Geophys. Res. Lett.*, 34(5), doi:10.1029/2006GL028139, 2007.
- Yager, E. M., Turowski, J. M., Rickenman, D. and McArdeell, B. W.: Sediment supply, grain protrusion, and bedload transport in mountain streams, *Geophys. Res. Lett.*, 39(10), 10402, doi:10.1029/2012GL051654, 2012.
- Yan, J., Zhang, M., Jung, J., Lin, Q., Zhao, S., Xu, S. and Chen, L.: Influence on the conversion of DMS to MSA and SO₄ 775 2⁻ in the Southern Ocean, Antarctica, *Atmos. Environ.*, 233, 117611, doi:10.1016/j.atmosenv.2020.117611, 2020.
- Zavarsky, A., Goddijn-Murphy, L., Steinhoff, T., & Marandino, C. A.: Bubble-mediated gas transfer and gas transfer suppression of DMS and CO₂. *J. Geophys. Res.*, 123, 6624–6647. <https://doi.org/10.1029/2017JD028071>, 2018.
- Zhang, M., Chen, L., Xu, G., Lin, Q. and Liang, M.: Linking phytoplankton activity in polynyas and sulfur aerosols over Zhongshan Station, East Antarctica, *J. Atmos. Sci.*, 72(12), 4629–4642, doi:10.1175/JAS-D-15-0094.1, 2015.
- 780 Zindler, C., Marandino, C. A., Bange, H. W., Schütte, F. and Saltzman, E. S.: Nutrient availability determines dimethyl sulfide and isoprene distribution in the eastern Atlantic Ocean, *Geophys. Res. Lett.*, 41(9), 3181–3188, doi:10.1002/2014GL059547, 2014.